CHALMERS

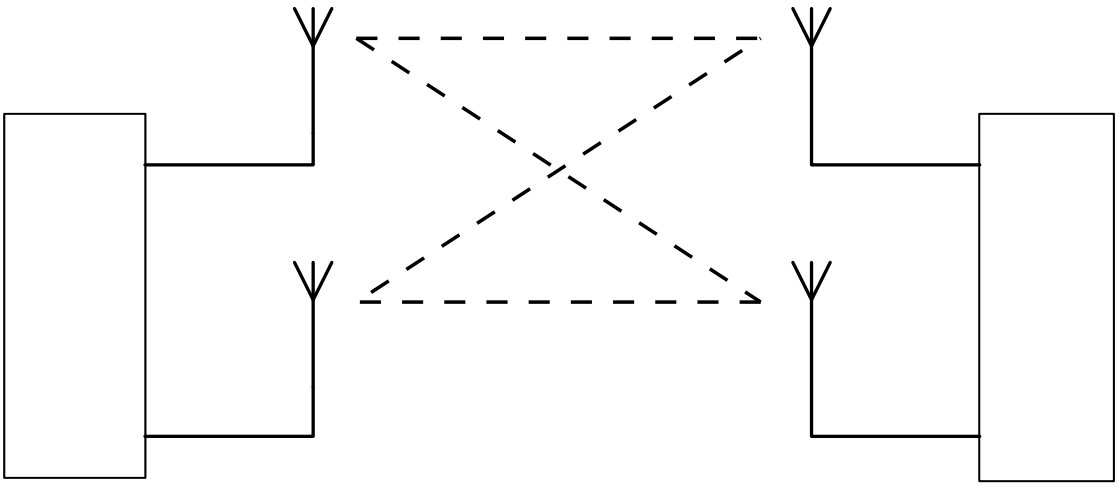

Measurements and Channel Modelling of Microwave Line-of-Sight MIMO Links

Master's Thesis in Communication Engineering

KARL RUNDSTEDT

Department of Signals & Systems
Chalmers University of Technology
Gothenburg, Sweden 2015
Master's Thesis EX007/2015

Measurements and Channel Modelling of Microwave Line-of-Sight MIMO Links

Master's Thesis in Communication Engineering

KARL RUNDSTEDT

CHALMERS
UNIVERSITY OF TECHNOLOGY

Department of Signals and Systems
Chalmers University of Technology
Gothenburg, Sweden 2015
Master's Thesis EX007/2015

Microwave Line-of-Sight MIMO Measurements and Channel Modelling
Master's Thesis in Communication Engineering
KARL RUNDSTEDT

Master's Thesis EX007/2015
Department of Signals and Systems
Chalmers University of Technology
SE-412 96 Gothenburg
Sweden
Telephone +46(0)31-772 10 00

Cover:
Schematic figure over a 2×2 MIMO system.

Chalmers University of Technology
Gothenburg, Sweden 2015

Abstract

The fading characteristics during meteorological conditions such as rain and variations of the atmospheric refractivity for Line-of-Sight (LOS) Multiple-Input-Multiple-Output (MIMO) channels are investigated. Measurements have been performed on two prototype LOS-MIMO links in Gothenburg, Sweden. It is showed that rain can be modelled as a fully correlated attenuation of the received MIMO signal. Refractive fading, caused by variations of the atmospheric refractivity, can be modelled as correlated multipath fading and especially as Rician fading. Later in the thesis, we investigated the performance and outage probability of LOS-MIMO systems compared to conventional Single-Input-Single- Output (SISO) systems in a Rician channal. Two MIMO systems are analyzed, a linear zero-forcing (ZF) system and an optimal (capacity-achieving) system using Singular Value Decomposition (SVD) of the channel. It is shown from simulation that an SVD system offers lower or equal outage probability than its SISO counterpart while the ZF system introduces a power penalty offset, given an equal probability of outage.

Keywords: LOS-MIMO channel model, LOS-MIMO outdoor measurements, LOS-MIMO outage probability

Acknowledgements

I would like to take this opportunity to give a special thank to Lei Bao from Ericsson and Rajet Krishnan from Chalmers for helping and supporting me in this project as my supervisors. I would like to thank Thomas Eriksson and Jonas Hansryd for giving many good advises and helpful comments, Bengt-Erik Olsson, Per Ligander and everyone at Ericsson who made the MIMO link measurements possible. Last but not least I want to thank my family and my fellow friends at Chalmers for your support throughout my work.

Karl Rundstedt, Göteborg August 2014

Contents

1

Introduction

In the past 10 years the world has experienced a technology revolution with the access to mobile broadband connections and connected devices. There is an ever increasing demand in the mobile networks for higher capacity, higher reliability and increased coverage and everything is expected to a reduced cost. Microwave links are one of the keystones of this development and the expansion of the mobile networks.

Microwave links provide fast and reliable connections in strong in addition to optical fiber connections. While microwave links still cannot match the capacity of an fiber connection, they offer a relatively cheap and flexible deployment to scenarios where fiber connections are not practical or much more expensive. As a result, a large portion of all radio base stations deployed today are connected via a microwave link to the core transport network. Operators and vendors struggle to provide faster connections and better user experience while keeping the cost down. By introducing multiple antennas at each terminals and using Multi-Input-Multi-Output (MIMO) technology on microwave links it is possible to double, triple or even further increase the capacity over the existing spectrum and thus minimizing the cost for new expensive fibre connections.

A disadvantage of microwave links is that they are affected by environmental conditions such as rain, atmospheric refraction, reflections etc. In current Single-Input-Single-Output (SISO) systems there exist several methods to predict the long term outage and capacity performance. But in the context of MIMO systems, methods to predict the performances under different weather conditions have not been studied. Models predicting statistical fading of MIMO microwave links will be crucial for designers to ensure that the capacity performance and availability of the links fulfil the required demands.

1.1 Problem Description

The main goals of this project were to evaluate statistical availability models for Line-of-Sight MIMO microwave links. The following tasks where identified as important prior to the work.

(i) Study prior work including scientific literature and the International Telecommunication Union (ITU) recommendations.
(ii) Investigate theoretical channel models for long term (propagation model) and short term channel effects (due to rain and refractive fading).
(iii) Investigate theoretically how the system performance is affected, independent of specific details of the transmitter-receivers that are employed in Ericsson systems.
(iv) Based on the knowledge gathered in tasks (i) and (ii), investigate how specific receiver structures such as those used by Ericsson impact LOS-MIMO performance and availability.
(v) Investigate how the study can be made relevant with respect to existing standards like those from ITU.

Analysis of real-world measurements from two experimental LOS-MIMO links deployed by Ericsson has been used to understand how MIMO technology impacts real performance of microwave links. A key focus during the work has been to gain a broad understanding of both theoretical and practical problems of designing an LOS-MIMO system.

1.2 Thesis Outline

In Chapter 2 an overview of current LOS microwave systems is provided. A brief introduction to microwave communications and key design parameters are explained. Chapter 3 explains MIMO technology and discusses how LOS-MIMO can be implemented. Important performance parameters are also introduced and discussed here. Chapter 4 gives a theoretical overview of microwave propagation. In Chapter 5 availability models and prediction methods for both long term and short term channel variations are discussed. Chapter 6 presents the LOS-MIMO test systems and measurement results. Chapter 7 presents an analysis on the performance of MIMO systems for short term channel variations. Chapter 8 discusses the main results of this thesis while Chapter 9 provides a final summary and conclusions.

1.3 Abbreviations and Acronyms

AWGN	Additive White Gaussian Noise
BER	Bit Error Rate
CDF	Cumulative Distribution Function
CSI	Channel State Information
CSIT	Channel State Information at the Transmitter
FEC	Forward Error Correction
ISI	Inter-Symbol-Interference
ITU	International Telecommunication Union
LOS	Line-Of-Sight
LTE	Long Term Evolution
MIMO	Multiple-Input-Multiple-Output
NLOS	Non-Line-Of-Sight
QAM	Quadrature Amplitude Modulation
SISO	Single-Input-Single-Output
SNR	Signal-to-Noise Ratio
SVD	Singular Value Decomposition
ZF	Zero-Forcing

A	fade depth attenuation
$A_{0.01}$	rain attenuation exceeded 0.01% of time
$\mathbf{B}$	ZF receiver matrix
$\mathbf{b}_k$	kth row of the receiver matrix $\mathbf{B}$
C	channel capacity
d_t	transmitting antenna separation
d_r	receiving antenna separation
f	carrier frequency
$\mathbf{H}$	Channel matrix
$\mathbf{H}_{\text{LOS}}$	LOS channel matrix component
$\mathbf{H}_{\text{NLOS}}$	NLOS channel matrix component
$\mathbf{h}_k$	kth column of H
h_{kl}	impulse response between the lth transmitting and kth receiving antenna
$\mathbf{I}$	identity matrix
K	geoclimatic factor
k_{earth}	effective earth radius
M	number of transmitting antennas
N	number of receiving antennas
N_0	noise spectral density
n	refractive index
P	transmitted power
P_{out}	outage probability
p_0	multipath occurrence factor
$\mathbf{Q}$	MIMO covariance matrix
$\mathbf{Q}_{\text{NLOS}}$	MIMO covariance matrix for of $\mathbf{H}_{\text{NLOS}}$
R	link hop length
r_{ij}	geometrical distance between the jth transmitting and ith receiving antenna
r_{eff}	effective rain distance
$\mathbf{S}$	power allocation matrix
$\mathbf{w}$	AWGN vector
$\mathbf{y}$	channel output vector

$\Delta\theta$	MIMO phase (3.15)
τ_{ij}	propagation time between the jth transmitting and ith receiving antenna
η	deployment number (3.14)
λ	wave length
γ	system penalty
γ_{SVD}	system penalty for a SVD-MIMO system
γ_{ZF}	system penalty for a ZF-MIMO system
γ_{R}	specific rain attenuation
ρ	correlation coefficient
Σ	MIMO path correlation matrix

.

2

Microwave Systems

Microwave links are accurately referred to as fixed point-to-point wireless communication systems using microwave frequencies. They are widely used by operators and vendors to build up backhaul communication networks to connect base stations with the core network. This is in contrast to fronthaul solutions aimed at connecting mobile users. A simple set-up of a microwave link is shown in Fig 2.1. It consists of a transmitter, receiver and two antennas. The channel can be considered as a random medium where different weather conditions can introduce random changes.

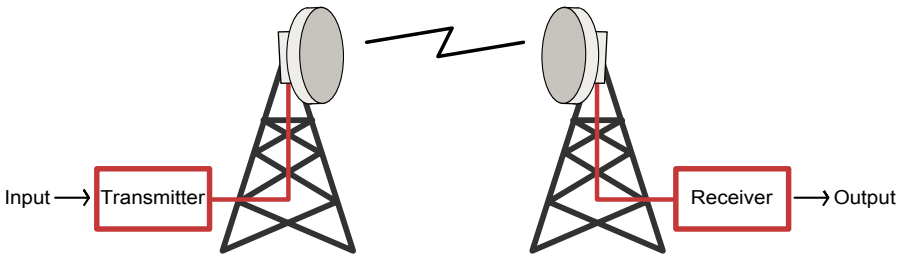

Figure 2.1: An simplified illustration of a line-of-sight microwave link.

Microwave links usually employ large bandwidths, up to 56MHz or more, enabling them to transmit large amount of data at high speed [1]. They are also relatively easy and inexpensive to deploy which makes them suitable to build up large networks [2, 3]. In the past, these networks have mainly been used to transmit cellular calls but today they are mainly used for the increasing data traffic.

As a result there is an increasing demand of higher capacity and reliability. Fiber connections are a strong competitor to provide high speed and reliable connections. The advantages of microwave links are mainly the inexpensive and flexible installation

which eliminates the need for any equipment, cables or installations between the two terminals. Microwave links can therefore easily be deployed almost anywhere as long as the terminals are within Line-of-Sight (LOS) and the distance within the system design specifications.

In order to compete with fiber networks the cost must be kept down while the capacity, reliability and flexibility must be increased. The availability is one of the most crucial factors for microwave links. A common industry standard is the so called 5-9's, which means the link must be operational 99.999% of the year. This corresponds to a downtime caused of about 5 minutes per year. The usual techniques to increase capacity while retaining availability include larger bandwidth, dual polarization, adaptive modulation and more recently also MIMO technology which is studied in this report.

2.1 System Overview

A block-diagram of Shannon's communication model is shown in Fig. 2.2. The source encoder formats the data prior to transmission. The channel encoder adds redundancy bits to the data before transmission over the unreliable, noisy channel. This is known as Forward Error Correction (FEC) coding. The third step involves modulation which maps the coded digital bit-stream into discrete symbols. The symbols is then filtered through a pulse-shaping filter into an analog signal which is then mixed with a carrier frequency and transmitted over the channel. The receiver has essentially all the steps of the transmitter but in reverse. The signal is mixed and filtered to be down-converted back to baseband. The baseband signal is sampled and passed to the demodulator, channel decoder and source decoder.

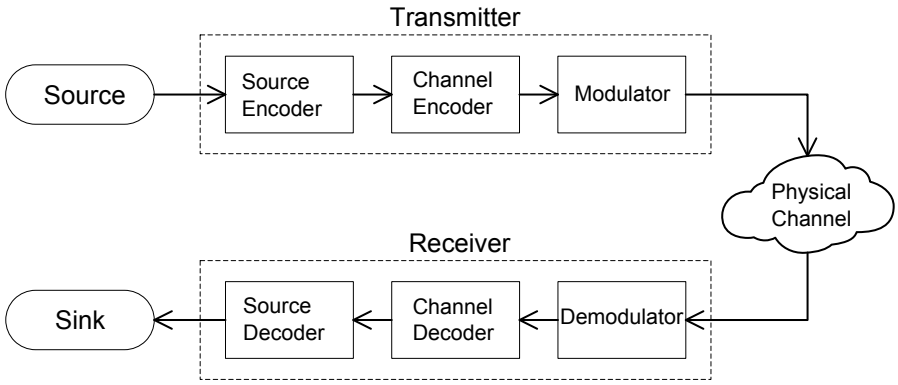

Figure 2.2: A block diagram of Shannon's communication model from 1948.

One of the most common modulation scheme for microwave system is called Quadrature Amplitude Modulation (QAM) where the information is encoded in both the amplitude and phase of a transmitted symbol. The full scheme is best represented in the complex plane with a so called signal constellation plot where each symbol represent a short bit

sequence. Noise in the system will result in an uncertainty of the mapping of the received symbols. More noise leads to an increased probability of errors during the detection and demodulation. However if the noise level is very low it is possible to correctly demodulate symbols that are very close to each other. This allows for constellation sizes of upto 4096-QAM symbols in current systems. Fig. 2.3 shows some QAM constellations of different sizes.

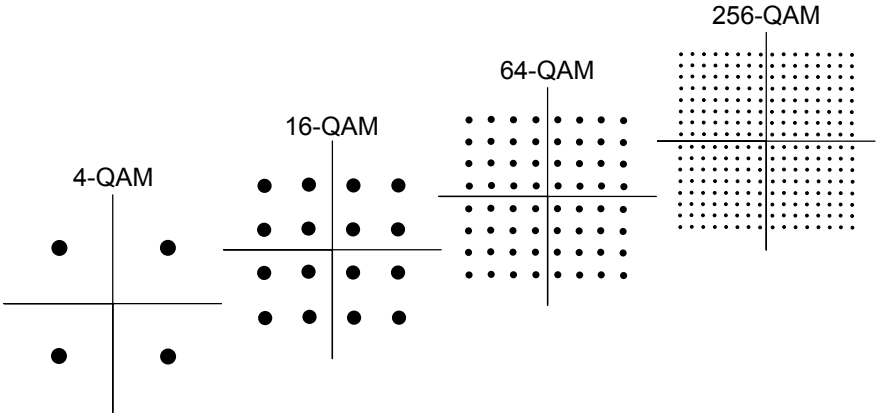

Figure 2.3: An illustrative figure over QAM signal constellations. The constallations are shown in an increasing order from 4-QAM to 256-QAM.

The bit-rate of the transmitted signal is dependent on the average number of transmitted bits per symbol and the symbol rate. Any overlay of the information bits such as channel coding will reduce actual information bit rate but most importantly it will also reduce the number of bit errors. The symbol rate is directly related to the spectrum bandwidth of the signal, wherefore larger bandwidths often means higher data rates.

2.1.1 Fading and Propagation Losses

Every signal that is transmitted wirelessly is subjected to noise and random channel variations due to fading and to attenuation due to propagation losses. The loss can usually be divided into a static loss from the free-space propagation and a random part from rain, refractive fading etc. Propagation and fading is presented in more detail in Chapter 4.

Fading effects are accounted for when planning a microwave link and the transmitted power must be large enough to compensate for the overall losses of the system. For this the concept of link budget is introduced. The link budget can include loss and gain from hardware such as wave guides, feeder, antennas and also free space loss. An example of a simple link budget could look like

$$P_{\mathrm{RX}} = P_{\mathrm{TX}} + G_{\mathrm{TX}} - L_{\mathrm{TX}} - L_{\mathrm{FS}} - L_{\mathrm{M}} + G_{\mathrm{RX}} - L_{\mathrm{RX}} \tag{2.1}$$

where P_{RX} is received power (dBm), P_{TX} is transmitted power (dBm), $G_{\mathrm{RX,TX}}$ are antenna gains (dBi), $L_{\mathrm{RX,TX}}$ are transmitter and receiver losses (dB), L_{FS} is the free-space loss (dB) and L_{M} are miscellaneous losses.

With the link budget in place the nominal received signal power level can be calculated by adjusting the transmit power. The margin between the nominal received signal level and the least acceptable level is called the fade margin. The fade margin is used to account for random fading of the received signal level. A large margin gives a more reliable system but will decrease the overall power efficiency and introduce more interference in dense networks. Many system can therefore adaptively change the transmit power level to increase the efficiency. A typical fade margin is usually around 30-40dB for a microwave link [1].

Several methods exist to calculate statistics of random fading. The method from ITU is often considered industry standard by operators and vendors. From this method the fade margin can be calculated for a given availability requirement. This method is presented in Chapter 5.

3

MIMO Systems

In this chapter we will introduce multiple antenna microwave systems and define the Multiple-Input-Multiple-Output (MIMO) system models used in this report. We will also present optimal channel conditions for LOS-MIMO systems and different matrices used to evaluate the system performance.

MIMO technology has attracted much attention over the last decade in almost all areas of wireless communication since it allows for increased capacity and reliability without additional power or bandwidth. Wireless spectrum is a valuable and limited resource, so in order to supply an increasing demand of higher capacity, MIMO has already been introduced in common wireless standards such as IEEE 801.11n, WiMAX and LTE.

When using MIMO technology, multiple receiving and transmitting antennas are used to increase capacity through spatial multiplexing without additional power or bandwidth. The capacity scales linearly with the minimum number antennas used at the transmitter or the receiver. With pre-coding of the signal it is also possible to spread the streams over all transmit antennas to obtain an additional array gain of the signal and/or simplify the receiver. In a fading channel the spatial diversity between the antennas can also be used to increase the average capacity and reduce the outage probability. Fig. 3.1 shows a schematic overview of a MIMO system.

While MIMO can improve almost every aspect of a wireless communication system, the multiple antenna design makes the systems more complex than single antenna systems. There are also practical problems with sufficient antenna separation for the MIMO systems to function optimally. Separation is generally not a problem for non-line-of-sight (NLOS) connections in a rich scattering environments i.e. typical conditions in access networks. However, MIMO technology has usually been considered unfavourable for LOS systems since the possible antenna separation has been considered to be too small to achieve any spatial multiplexing. However it has been shown that as the frequen-

cies increase, the minimum separation can be made smaller which has driven a recent development to introduce MIMO on microwave links [4, 5].

The next sections will handle narrowband MIMO system models and explain how the array gain and multiplexing gain are achieved. Conditions for LOS-MIMO systems will be presented and expressions for channel capacity and other performance parameters are also introduced.

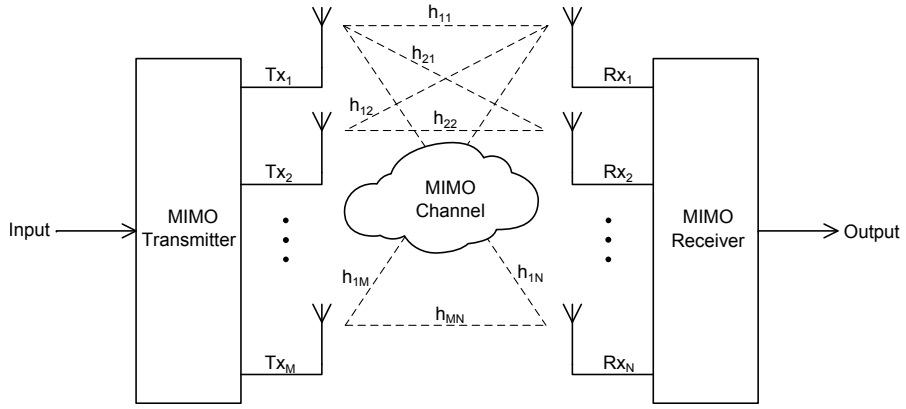

Figure 3.1: A schematic figure of a wireless MIMO system with M transmittning and N receiving antennas.

3.1 Narrowband MIMO Systems

A system is considered narrowband if the systems bandwidth does not exceed the channel's coherence bandwidth. In other words this means that the frequency response over the system bandwidth can be considered flat. Description and analysis of such a system are then greatly simplified. Variations over the frequency response are usually caused by delayed multipath components. A flat frequency response occurs if the symbol time T_s is much larger than the average multipath delay spread T_m, i.e. $T_s \gg T_m$.

A narrowband MIMO channel can be described by a channel matrix $\mathbf{H}$. The elements of $\mathbf{H}$ are complex numbers that represent the amplitude and phase shift introduced by the channel. A MIMO system is shown in Fig. 3.1 where the element h_{ij} represent the channel from the jth transmitting antenna to the ith receiving antenna.

In this report we will consider a MIMO system with equal number of transmitting and receiving antennas, $N_{\mathrm{Rx}} = N_{\mathrm{Tx}} = N$. This gives $N \times N$-MIMO channels and possibility to support up to N independent spatial data streams. The channel is assumed to be slow varying and frequency flat as has shown to be the case in most short to medium haul links with hop lengths less than 20km [1, 3]. The received signal is modelled as

$$\mathbf{y} = \mathbf{H}\mathbf{x} + \mathbf{w} \tag{3.1}$$

where $\mathbf{y}$ is the $N \times 1$ channel output vector, $\mathbf{H}$ is the $N \times N$ channel matrix, $\mathbf{x}$ is the $N \times 1$ transmitted signal vector and $\mathbf{w}$ is a $N \times 1$ complex additive white Gaussian noise (AWGN) vector that represent signal noise in the system. The system is normalized for the free-space loss of a real channel, meaning that each element has unit average power.

Two different MIMO systems will be considered. The first system is a capacity-optimal system achieved by parallel decomposition of the MIMO channel, also known as eigenmode transmission. The second system is a linear Zero-Forcing (ZF) system. The ZF system is used as a practical case as the system structure is simple and the performance with respect to capacity is optimal if the MIMO channel is of full rank, meaning that the signal streams directly can be transmitted in orthogonal sub-channels [6].

3.1.1 Eigenmode Transmission System

If channel state information (CSI) is assumed to be available at both the transmitter and receiver, a capacity-optimal MIMO system is here given by a parallel decomposition of the MIMO system [6]. Any channel matrix $\mathbf{H}$ can be expressed using its singular value decomposition (SVD) as

$$\mathbf{H} = \mathbf{U}\mathbf{D}\mathbf{V}^* \tag{3.2}$$

where $\mathbf{U}$ and $\mathbf{V}$ are $N \times N$ unitary matrices while $\mathbf{D}$ is a diagonal matrix of singular values d_i of $\mathbf{H}$. The operator $(\cdot)^*$ represents the hermitian transpose. Parallel decomposition is accomplished by precoding the transmitter input $\tilde{\mathbf{x}}$ with $\mathbf{V}$ as $\mathbf{x} = \mathbf{V}\tilde{\mathbf{x}}$. This results in transmission over parallel and orthogonal sub-channels. At the channel output there is a similar operation called receiver shaping that is achieved by multiplying the channel output $\mathbf{y}$ with $\mathbf{U}^*$ as $\tilde{\mathbf{y}} = \mathbf{U}^*\mathbf{y}$ where $\tilde{\mathbf{y}}$ is the received signal vector. Optimal rate of the system can be achieved by introducing power allocation on the parallel sub-channels. This is modelled by multiplying $\tilde{\mathbf{x}}$ with a $N \times N$ diagonal power allocation matrix $\mathbf{S}$. We get the following expression for the MIMO transmission

$$\begin{aligned} \tilde{\mathbf{y}} &= \mathbf{U}^*(\mathbf{H}\mathbf{x} + \mathbf{w}) \\ &= \mathbf{U}^*(\mathbf{U}\mathbf{D}\mathbf{V}^*\mathbf{x} + \mathbf{w}) \\ &= \mathbf{U}^*(\mathbf{U}\mathbf{D}\mathbf{V}^*(\mathbf{V}\mathbf{S}\tilde{\mathbf{x}}) + \mathbf{w}) \\ &= \mathbf{D}\mathbf{S}\tilde{\mathbf{x}} + \tilde{\mathbf{w}} \end{aligned} \tag{3.3}$$

where $\tilde{\mathbf{w}}$ is AWGN with equal distribution as $\mathbf{w}$ after the unitary projection. The diagonal elements of the $\mathbf{S}$ are optimally given water filling power allocation [6] and must satisfy the total transmitted power condition

$$\sum_{n=1}^{N} s_n = N. \tag{3.4}$$

The symbol s_i denotes the diagonal elements of $\mathbf{S}$ and are given by (3.5) for $i = 1, \ldots, N$ as

$$s_n = \left(\xi - \frac{1}{N_0 d_n^2}\right)^+. \tag{3.5}$$

The parameter ξ is chosen so that the total transmitted power condition is satisfied. The operator $(\cdot)^+$ is zero if its argument is negative. Finally, the symbol N_0 denotes the noise spectral density [W/Hz] of the channel.

3.1.2 Zero-Forcing System

A linear receiver with only receiver CSI can be modelled by multiplying $\mathbf{y}$ with a receiver matrix $\mathbf{B}$. For a ZF receiver $\mathbf{B}$ is given by the inverse of the channel $\mathbf{B} = \mathbf{H}^{-1}$ if $\mathbf{H}$ is of full rank. If the rank of $\mathbf{H}$ is deficient the pseudo inverse of the channel may be used instead as

$$\mathbf{B} = (\mathbf{H}^*\mathbf{H})^{-1}\mathbf{H}^*. \tag{3.6}$$

In this case one data stream is transmitted per transmitting antenna. The rank of the channel $\mathbf{H}$ must be larger or equal to the number of data stream for the zero-forcing operation to be successful. Hence, the transmission over ZF-MIMO system can be expressed by (3.7).

$$\begin{aligned} \tilde{\mathbf{y}}_{\mathrm{ZF}} &= \mathbf{B}\mathbf{y} \\ &= \mathbf{B}(\mathbf{H}\mathbf{x} + \mathbf{w}) \\ &= \mathbf{x} + \tilde{\mathbf{w}}_{\mathrm{ZF}} \end{aligned} \tag{3.7}$$

where $\tilde{\mathbf{y}}_{\mathrm{ZF}}$ is the received signal vector and $\tilde{\mathbf{w}}_{\mathrm{ZF}}$ is scaled AWGN after projection

3.2 Line-of-Sight MIMO Systems

In this section geometrical deployment conditions for pure Line-of-Sight MIMO systems will be presented. Optimal deployment in terms of channel capacity for linear antenna arrays has been treated by [5, 7] where it was shown that the geometrical distance and

delay of the MIMO paths determine the rank of the channel $\mathbf{H}_{\text{LOS}}$. The channel is assumed to be narrowband, deterministic and subjected to AWGN.

A linear antenna array is considered as in Fig. 3.2. The channel matrix is a function of the carrier frequency f and the propagation time τ_{nm} between each pair of receiving and transmitting antennas, hence $n,m \in [1,N]$. The small difference in distance between the MIMO paths can be derived from a planar wave approximation. The gain of all paths are equal from the far-field assumption and normalized to one. The channel matrix for a MIMO system can then be expressed as

$$\mathbf{H}_{\text{LOS}} = \begin{bmatrix} h_{11} & \cdots & h_{1N} \\ \vdots & \ddots & \vdots \\ h_{N1} & \cdots & h_{NN} \end{bmatrix} = \begin{bmatrix} e^{(j2\pi f\tau_{11})} & \cdots & e^{(j2\pi f\tau_{1N})} \\ \vdots & \ddots & \vdots \\ e^{(j2\pi f\tau_{N1})} & \cdots & e^{(j2\pi f\tau_{NN})} \end{bmatrix}. \tag{3.8}$$

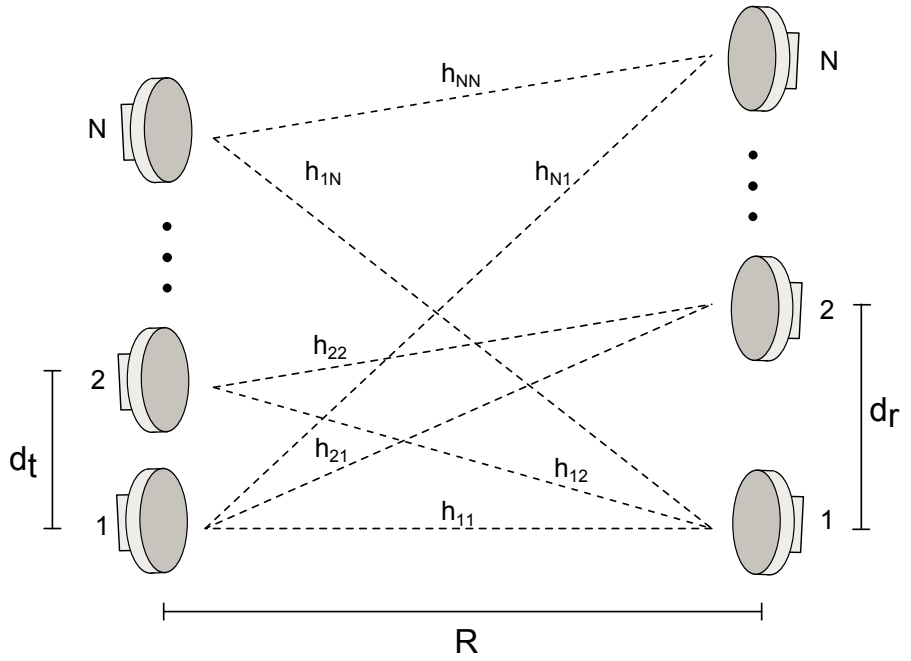

Figure 3.2: Illustration of rectangular LOS-MIMO system setup. The geometrical between the antennas determin the rank of the channel.

For the normalized MIMO channel where all signals have equal strength the channel is optimal in terms of channel capacity if all rows or columns are orthogonal, $\langle \mathbf{h}_k, \mathbf{h}_l \rangle = 0$ for $k,l \in [1,N]$. The $N \times 1$ vectors $\mathbf{h}_k$ and $\mathbf{h}_l$ represent the kth and lth column of the channel matrix. Now consider $\mathbf{H} = \mathbf{H}_{\text{LOS}}$ the channel optimality condition is given by

$$\begin{aligned}\langle \mathbf{h}_k, \mathbf{h}_l \rangle &= \sum_{n=1}^{N} e^{(j2\pi f[\tau_{nk}-\tau_{nl}])} \\ &= \sum_{n=1}^{N} e^{\left(j\frac{2\pi}{\lambda}[r_{nk}-r_{nl}]\right)} \\ &= \sum_{n=1}^{N} e^{(j2\pi[\angle h_{nk}-\angle h_{nl}])} = 0\end{aligned} \tag{3.9}$$

where r_{nm} is the geometrical distance from the mth transmitting antenna to the nth receiving antenna, λ is the wavelength and $\angle$ is the angle operation. For a linear antenna array, the optimality condition can easily be satisfied by a careful deployment. The distances r_{nm} are given from the geometrical deployment and can be calculated from

$$r_{nm} = \sqrt{R^2 + (nd_r - md_t)^2} \approx R\left(1 + \frac{(nd_r - md_t)^2}{2R^2}\right) = \frac{-nmd_rd_t}{R} + \frac{n^2d_r^2 - m^2d_t^2}{2R} + R \tag{3.10}$$

where d_t and d_r are the antenna separation along a common axis normal to the hop direction for the transmitter respective receiver and R is the hop length. Since $d << R$ the distances can be approximated from the first order Taylor expansion. The path difference between antenna pairs is given by

$$r_{nk} - r_{nl} = \frac{(l-k)\, nd_rd_t}{R} + \frac{(k^2 - l^2)\, d_t^2}{2R}. \tag{3.11}$$

The second term $\frac{(k^2-l^2)d_t^2}{R}$ only introduce a common phase shift which does not change the orthogonality. This gives the resulting condition

$$\langle \mathbf{h}_k, \mathbf{h}_l \rangle = \sum_{n=1}^{N} e^{\left(j2\pi\frac{d_td_r}{\lambda R}(l-k)n\right)} = 0. \tag{3.12}$$

By solving this equation subjected to the antenna separation distances it yields the solution corresponding to the smallest separations as

$$d_td_r = \frac{\lambda R}{N}. \tag{3.13}$$

So far the antenna array setup has been assumed to be parallel but the idea can easily be extended to non-rectangular setup. It was shown by [4] that every linear array setup can

be projected on virtual parallel array for which the given optimality expression (3.13) is valid. For a linear array, the optimality condition of (3.12) can be simplified in terms of deployment specific parameters to give the the deployment number η as in

$$\eta = \sqrt{\frac{d_t d_r}{\lambda R} N}. \tag{3.14}$$

The channel deployment is optimal if $\eta = 1$ and a sub-optimal deployment will result in reduced channel capacity.

3.2.1 Alternative Optimality Conditions

In the case of 2×2-MIMO system the capacity optimality condition of the channel can be be related to the relative phase differences of the MIMO paths as in

$$\Delta\theta = (\angle h_{11} - \angle h_{12}) + (\angle h_{21} - \angle h_{22}) - \pi \tag{3.15}$$

where we introduce $\Delta\theta$ as the MIMO phase. The expression is related to the orthogonality conditions in (3.9) by

$$\langle \mathbf{h}_1, \mathbf{h}_2 \rangle = e^{(j2\pi[\angle h_{11} - \angle h_{12}])} + e^{(j2\pi[\angle h_{21} - \angle h_{22}])} = 0. \tag{3.16}$$

The MIMO phase $\Delta\theta$ is introduced as a parameter to measure optimal deployment conditions and channel orthogonality in real systems. Later it is also used to measure uncorrelated phase variations of the MIMO paths during channel fading. In terms of deployment parameters, $\Delta\theta$ becomes (3.17)

$$\Delta\theta = 2\pi \frac{d_t d_r}{\lambda R} - \pi \tag{3.17}$$

where the optimal value is given by $\Delta\theta_{\text{Opt}} = 0$.

3.3 Performance Measures

A various number of parameters can be used to characterize the performance of a MIMO system, such as channel capacity and outage probability. Channel capacity is a well studied limit and a widely used measure to analyse fundamental data rate limit of a system. Outage probability is defined for a specific system as the probability that a transmission over the channel is not possible. However most practical systems operate below the theoretical limits due to hardware limitations, receiver complexity and channel

variations. Most systems are limited by power and therefore system penalty γ is also introduced in this section, as an equivalent to fade attenuation of SISO systems. The system penalty can also be used to define outage probabilities,

3.3.1 Capacity

Ergodic Capacity of the SVD-MIMO system with full CSI and parallel decomposition of the MIMO channel is given by

$$C = \mathbb{E}\left[\log_2 \det(\mathbf{I}_N + \frac{P}{N_0 N}\mathbf{HQH}^*)\right] \text{[bits/s/Hz]}. \tag{3.18}$$

The capacity of a ZF-MIMO receiver is given by

$$C = \mathbb{E}\left[\sum_{k=1}^{N} \log_2\left(1 + \frac{P/N}{N_0\|\mathbf{b}_k\|^2}\right)\right] \text{[bits/s/Hz]}. \tag{3.19}$$

as the sum of the capacity of the output signal streams [6]. The operator $\mathbb{E}$ represents the expected value, $\det(\cdot)$ is the determinant, $\mathbf{H}$ is the $N \times N$ channel matrix, $\mathbf{I}_N$ is the $N \times N$ identity matrix, P is the total transmitted power, N_0 is the noise spectral density and $\mathbf{Q}$ denotes the signal covariance given by parallel channel decomposition and water-filling power allocation as $\mathbf{Q} = \mathbf{VSV}^*$ [6]. In addition, $\|\cdot\|$ is the Euclidean norm. The vector $\mathbf{b}_k$ is the kth row of the receiver matrix $\mathbf{B}$.

The ergodic capacity is given from the time average of the instantaneous capacity. Capacity is a good measure for random fast varying channels. However the measure is not appropriate for determining the quality or outage probability of a random channel that are caused by fast deviation from the average signal level. For narrow-band channel the ergodic capacity means the expected time averaged capacity. For a slow-varying or deterministic channel ergodic and instantaneous capacity are equal. A common constraint in MIMO systems is the absence of channel state information at the transmitter (CSIT). A capacity optimal transmission is then achieved by allocating equal power on each spatial stream which gives the covariance matrix $\mathbf{Q} = \mathbf{I}$ [8]. The capacity is given by

$$C = \mathbb{E}\left[\log_2 \det(\mathbf{I} + \frac{P}{N_0 N}\mathbf{HH}^*)\right] \text{[bits/s/Hz]}. \tag{3.20}$$

3.3.2 System Penalty

Microwave links are often associated with a fade margin wherefore a larger fade will result in a system breakdown. While a fade margin cannot directly be applied on a

MIMO system, the concept of penalty has previously been introduced by [9] and others. Here it is defined as the power needed to restore the capacity given a channel $\mathbf{H}$ to that of normalized LOS channel $\mathbf{H}_{\text{LOS}}$. Similarly the penalty of the ZF receiver is also defined from the capacity of the system. A ZF system transmits several independent signal streams and the performance is largely dependent on the worst stream. The system penalty is defined as the power needed to restore the capacity of the worst stream. In real microwave systems penalty can also be defined as the power given to restore a given bit error rate (BER) for a fixed throughput. This definition is dependent on the specific implementation and beyond the scope of this report to study in detail.

For the system penalty derivation we use a high SNR approximation of the capacity for simplification and as microwave link systems usually operates at high SNR [1]. The capacity under high SNR approximation is given by

$$C = \log_2 \det\left(\mathbf{I} + \frac{P}{N_0 N}\mathbf{H}\mathbf{Q}\mathbf{H}^*\right) \approx \log_2 \det\left(\frac{P}{N_0 N}\mathbf{H}\mathbf{Q}\mathbf{H}^*\right). \tag{3.21}$$

The asymptotic system penalty for high SNR for the SVD-MIMO system is defined as follows. The penalty is the ratio between transmitted power needed, P for $\mathbf{H}$ and P_{LOS} for $\mathbf{H}_{\text{LOS}}$ to fulfil the equal capacity condition $C = C_{\text{LOS}}$. The penalty for an SVD system γ_{SVD} is given by

$$\begin{aligned} C = C_{\text{LOS}} \Rightarrow \det\left(\frac{P}{N_0 N}\mathbf{H}\mathbf{Q}\mathbf{H}^*\right) &\approx \det\left(\frac{P_{LOS}}{N_0 N}\mathbf{H}_{\text{LOS}}\mathbf{Q}\mathbf{H}_{\text{LOS}}^*\right) \\ \Leftrightarrow P^N |\det(\mathbf{H})|^2 \det(\mathbf{Q}) &\approx P_{\text{LOS}}^N |\det(\mathbf{H}_{\text{LOS}})|^2 \det(\mathbf{Q}) \\ \Rightarrow \gamma_{\text{SVD}} \triangleq \frac{P}{P_{\text{LOS}}} &\approx \left[\frac{|\det(\mathbf{H}_{\text{LOS}})|}{|\det(\mathbf{H})|}\right]^{\frac{2}{N}} \end{aligned} \tag{3.22}$$

given the properties for $N \times N$ complex matrices; $\det(c\mathbf{A}) = c^N \det(\mathbf{A})$ where c is a scalar, $\det(\mathbf{AB}) = \det(\mathbf{A})\det(\mathbf{B})$ and $\det(\mathbf{AA}^*) = |\det(\mathbf{A})|^2$. The operator $|\cdot|$ represent the absolute value. The penalty to a full rank LOS channel where all columns are orthogonal can be simplified to

$$\gamma_{\text{SVD,opt}} \approx \frac{N}{|\det(\mathbf{H})|^{\frac{2}{N}}}. \tag{3.23}$$

The penalty for a ZF receiver is defined using the high SNR approximation as

$$C_k = \log_2\left(1 + \frac{P/N}{N_0\|\mathbf{b}_k\|^2}\right) \approx \log_2\left(\frac{P/N}{N_0\|\mathbf{b}_k\|^2}\right) \tag{3.24}$$

where C_k is the capacity of the signal stream transmitted from the kth antenna, $\mathbf{b}_k$ is the kth row of ZF receiver matrix $\mathbf{B}$ given the channel $\mathbf{H}$ and $k \in [1,N]$. The penalty for the ZF system γ_{ZF} is defined as the power needed to restore the capacity, $\min_k C_k$, of the worst stream given $\mathbf{H}$ to that of the worst stream capacity, $\min_k C_{\mathrm{LOS},k}$, of $\mathbf{H}_{\mathrm{LOS}}$. This is expressed as

$$\begin{aligned} \min_k C_k = \min_k C_{\mathrm{LOS},k} \Rightarrow \frac{P/N}{N_0 \max_k \|\mathbf{b}_k\|^2} &\approx \frac{P_{\mathrm{LOS}}/N}{N_0 \max_k \|\mathbf{b}_{\mathrm{LOS},k}\|^2} \\ \Rightarrow \gamma_{\mathrm{ZF}} \triangleq \frac{P}{P_{\mathrm{LOS}}} &\approx \frac{\max_k \|\mathbf{b}_{\mathrm{k}}\|^2}{\max_k \|\mathbf{b}_{\mathrm{LOS,k}}\|^2}. \end{aligned} \tag{3.25}$$

Again, the penalty to a full rank LOS channel where all columns are orthogonal can be simplified to

$$\gamma_{\mathrm{ZF,opt}} = N \max_k \|\mathbf{b}_k\|^2. \tag{3.26}$$

Outage: One of the most important properties of a microwave link is outage probability. The outage for a given system is here defined as the probability of a penalty larger than a penalty threshold. The penalty threshold is here related to the lowest acceptable capacity or worst stream capacity depending on the receiver structure. The outage probability is given by

$$P_{\mathrm{out}} = \Pr\left(\gamma > \gamma_{\mathrm{thr}}\right) \tag{3.27}$$

3.3.3 Capacity and System Penalty of Line-of-Sight MIMO systems

With the derived deployment number η for the channel $\mathbf{H}_{\mathrm{LOS}}$ (3.8) where all elements have unit power, it is straight forward to calculate the capacity and system penalty for any linear array deployment, given hop-length, antenna separation and frequency. From a design point-of-view it is interesting to see how the capacity and penalty are affected for non-optimal antenna separation and $\eta \neq 1$. For an easy deployment of the system, it is most often convenient to keep the separation as small as possible. For 2×2 MIMO system it is possible to derive closed forms expressions for the deployment penalty with respect to η in LOS channels. A simplified expression of (3.23) for a 2×2 SVD-MIMO system in a normalized LOS channel (3.8) is given by

$$\gamma_{\mathrm{SVD,2\times2,deployment}} \approx \left|\sin\left(\frac{\pi}{2}\eta^2\right)\right|^{-1}. \tag{3.28}$$

It can also be shown that a equivalent expression for a ZF-MIMO system derived from derived from (3.26) is given by

$$\gamma_{\mathrm{ZF},2\times2,\mathrm{deployment}} = \left|\sin\left(\frac{\pi}{2}\eta^2\right)\right|^{-2}. \tag{3.29}$$

Fig. 3.3a shows the variation of the penalty from (3.28) and (3.29), given the deployment number η. For this case, η is equal to the ratio between the actual antenna separation d and optimal antenna separation d_{opt} as $\eta = d/d_{\mathrm{opt}}$. One can show that for a 2×2 LOS-MIMO system, the penalty can also be related to the MIMO phase $\Delta\theta$ and equivalently a MIMO phase penalty.

Since the expression of η involves the product of the antenna separations at both transmitter and receiver, it is possible to alter d_t and d_r individually. For an intuitive understanding of sensitivity for deployment penalty, the penalty is plotted against both d_t and d_r in Fig. 3.4. for the ZF-MIMO system. As seen, relatively big changes for d_t and d_r can be allowed at a small penalty.

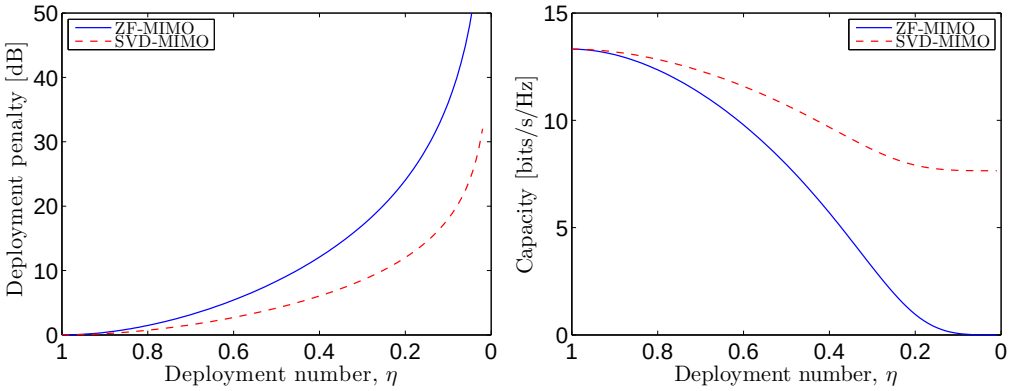

(a) The system penalty against η. **(b)** The capacity against η at SNR=20dB

Figure 3.3: The system penalty and capacity for both 2×2 ZF-MIMO and SVD-MIMO system plotted against the deployment number η.

It is seen from Fig. 3.3 that for $\eta > 0.7$ the capacity loss is small and the penalty for both systems is kept under $\gamma_{\mathrm{ZF}} < 3$ dB. When $\eta = 1$ it can be showed that the capacity of both systems is given by

$$C_{max} = N \log_2\left(1 + \frac{P}{N_0}\right). \tag{3.30}$$

Given a total transmitted power constrain P the capacity is related to that of a SISO system multiplied with the number of spatial streams, N. As the separation decreases the capacity is reduced and penalty increases for both systems. The signal subspaces will no longer be orthogonal which will cause interference between the spatial streams. When $\eta = 0$, $\mathbf{H}_{\mathrm{LOS}}$ becomes of rank 1 and will only support one spatial stream. For the

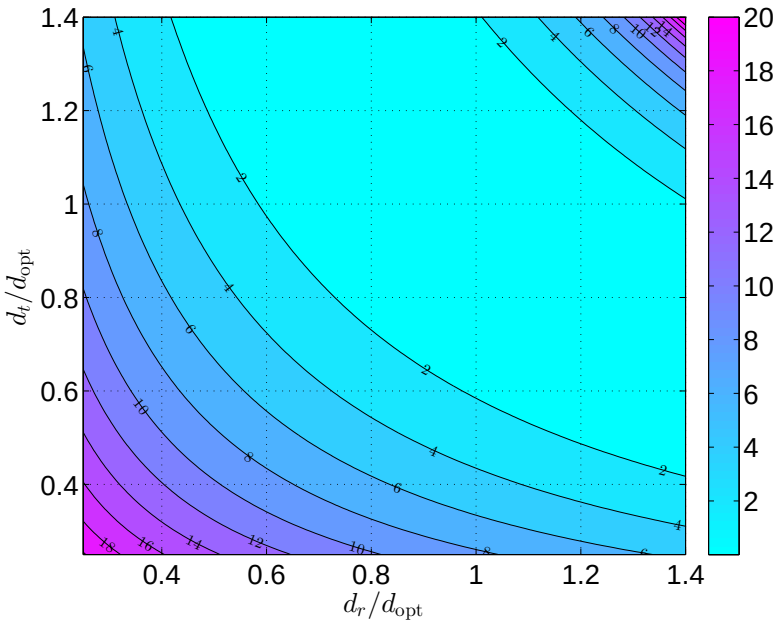

Figure 3.4: System penalty [dB] for a 2×2 ZF-MIMO system against sub-optimal antenna separation.

SVD-MIMO system, the capacity approaches that of a SISO system but with additional array gain from both the transmitter and receiver as

$$C_{min} = \log_2 \left(1 + N^2 \frac{P}{N_0} \right). \tag{3.31}$$

However, for the ZF-MIMO system the capacity approaches zero since the channel only will support a single stream and interference cancellation is not possible. The penalty therefore approaches infinity.

3.4 Wideband MIMO Systems

A system is considered wideband if the mean delay spread of the signal τ_m is smaller that the symbol time T_s. In time domain this will result in symbol dispersion and thus inter-symbol-interference (ISI). In the frequency domain it results in a non-flat spectrum. At the receiver this requires additional functions to manage the problem. The most common technique is called equalizing for which the name implies the spectrum is equalized and ISI is removed. The operation can be performed in both time and frequency domain.

3.4.1 Performance

The ergodic capacity of a wide band MIMO system is given by maximizing the rate by allocate transmitted power over both spatial and frequency dimensions as in

$$C = \mathbb{E}\left[\sum_{n=1}^{N} \int \log_2\left(1 + \frac{P s_n(f)}{N N_0} d_n(f)^2\right) \mathrm{d}f\right] \tag{3.32}$$

where $s_i(f)$ represent the power allocated to the ith transmitted signal at frequency f and $d_i(f)$ is the singular value of the channel matrix $\mathbf{H}(f)$ at frequency f. Each spatial frequency selective channel can be seen as set of flat-fading sub-channels. Then the capacity is the sum of the capacity in the sub-channels subjected to a total power constraint. The optimal power allocation given CSIT is achieved with water-filling and equal allocation if CSIT is not available [6, 8]. The solution to the water-filling approach is given by solving

$$s_n(f) = \left(\xi - \frac{1}{N_0 d_n(f)^2}\right)^+, \sum_{n=1}^{N} \int s_n(f) \mathrm{d}f \leq N. \tag{3.33}$$

where $(\cdot)^+$ is zero if its argument is negative. For an unknown channel at the transmitter (no-CSIT) the capacity is given by

$$C = \mathbb{E}\left[\sum_{n=1}^{N} \int \log_2\left(1 + \frac{P}{N N_0} d_n(f)^2\right) \mathrm{d}f\right]. \tag{3.34}$$

The penalty for a wide band system can be defined as for the narrowband system, as the power needed to restore capacity. However describing the penalty analytically in the same way as in the narrowband channel is intractable.

3.5 Summary of Capacity and Penalty Expressions

Some important capacity expression used in this report are summarized in Tab. 3.1 while penalty expressions are summarized in Tab. 3.2.

Table 3.1: Summary of capacity expressions in narrowband MIMO systems

Capacity description	Expression
Ergodic, SVD-MIMO	$C = \mathbb{E}\left[\log_2 \det(\mathbf{I}_N + \frac{P}{N_0 N}\mathbf{H}\mathbf{Q}\mathbf{H}^*)\right]$ (3.18)
Ergodic, ZF-MIMO	$C = \mathbb{E}\left[\sum_{k=1}^{N} \log_2\left(1 + \frac{P/N}{N_0 \|\mathbf{b}_k\|^2}\right)\right]$ (3.19)
Optimal, full rank LOS channel (3.9)	$C = N \log_2\left(1 + \frac{P}{N_0}\right)$ (3.30)

Table 3.2: Summary of asymptotic system penalty expressions for high SNR to an optimal LOS channel.

Description	Expression
SVD system penalty	$\gamma_{\text{SVD,opt}} \approx \frac{N}{\lvert\det(\mathbf{H})\rvert^{\frac{2}{N}}}$
ZF system penalty	$\gamma_{\text{ZF,opt}} = N \max_k \|\mathbf{b}_k\|^2$
2×2 SVD deployment penalty	$\gamma_{\text{SVD},2\times2,\text{deployment}} \approx \left\lvert\sin\left(\frac{\pi}{2}\eta^2\right)\right\rvert^{-1}$
2×2 ZF deployment penalty	$\gamma_{\text{ZF},2\times2,\text{deployment}} = \left\lvert\sin\left(\frac{\pi}{2}\eta^2\right)\right\rvert^{-2}$

4

Microwave Propagation

In this chapter we will present a theoretical overview of microwave propagation. We will also explain the most important phenomenas that contribute to the fading on microwave links.

For any given wireless link the signal will experience various propagation losses including the free-space loss. The channel between the two terminals can be considered as a random medium affecting the signal and hence the performance of the link. For a longer hop, the signal will pass through more random media and be more affected by random changes. This may cause big degradation in the performance. Physical effects are generally grouped into two different categories; precipitation and clear-air effects. precipitation effects are attenuation due to rain, fog and snow. In this report, clear-air effects is referred to as refractive fading effects and are caused by changes in the refractive index in the atmosphere. Changes in the refractive index will cause the ray or wave front to bend and diverge from the nominal path.

Rain and refractive fading are usually considered as independent events [2] and the severity of the fading is both dependent on the frequency and the hop length. The frequency used in most microwave systems ranges typically from 4 to 38GHz mainly depending on hop-length and available spectrum [1]. As a rule of thumb microwave links are often categorized in short-haul (0 to 15km), medium-haul (15-30km) and long-haul (30-150km) installations. Long-haul links often operate at lower frequencies between 4-13GHz as those are less attenuated by rain. But longer hop-lengths also increase the probability for refractive fading. Short-haul links usually do not suffer from refractive fading but are instead more sensitive to rain fading because higher frequencies are usually used. Higher frequencies are usually preferred due to available spectrum and benefits of smaller antennas with larger directivity. As a result short-haul links are usually limited by rain while long-haul links are limited by refractive fading. Recently, links operating

in the E-band (70-90GHz) or even higher frequencies have been investigated. This allows for short but high capacity links since the available spectrum is large.

Both rain and refractive fading depend strongly on climatic factors and both effects often needs to be taken into account when planning a link. This section will in more detail describe rain and refractive fading.

4.1 Rain fading

It is well known that rain will attenuate the overall signal power level of a microwave link. This is mainly because of scatter caused by the rain droplets but also due to dielectric losses. The loss is related to the rain rate and the relation between droplet size and the wavelength. In general, shorter wavelengths are more attenuated and for frequencies below 5GHz the attenuation can usually be ignored. There is also a small difference in attenuation between horizontal and vertical polarized signal due to the slightly flat shape of water droplets caused by the wind resistance. Fig. 4.1 shows the attenuation caused by rain against the frequency for different rain rates. A well-known empirical formula of rain attenuation from ITU is given as

$$\gamma_{\mathrm{R}} = kR_{\mathrm{rain}}^{\alpha} \tag{4.1}$$

where R_{rain} is the rain rate [mm/h]. The coefficients k and α are frequency and polarization dependent parameters which can be calculated or given from tables provided by ITU [10].

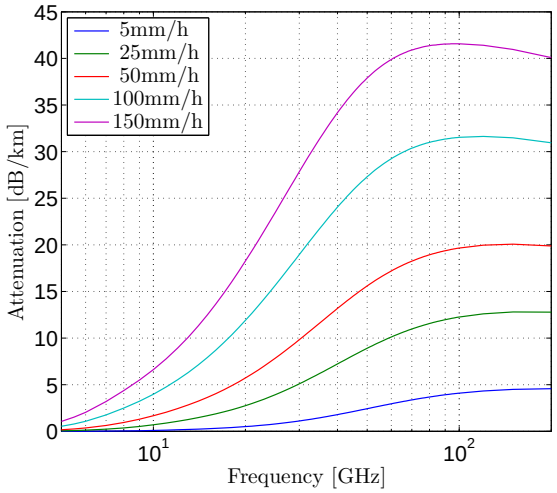

Figure 4.1: Rain attenuation for horizontal polarization against frequency for different rain rates.

Another effect caused by rain is depolarization which can give problems to systems using dual polarizations to transmit independent signals. Polarization distortions affect the system's ability to separate the signals at the receiver based on their polarization. In addition, rain may also change the properties of reflecting surfaces. A wet surface often has increased conductivity which can increase reflections and scatter. It has been shown that links partly obstructed by vegetation can experience increased scatter during rain [11].

4.2 Refractive Fading

The atmosphere is not a homogeneous media as often approximated. Properties, such as temperature, humidity and pressure of the air will change over both space and time. These properties will also change the refractive properties of the atmosphere. Refractive fading can be characterized into several different effects with different fading properties. In this section we present the most significant effects such as diffraction loss, defocusing/ducting and multipath fading, also presented in Tab. 4.1.

Table 4.1: Overview of refractive fading effects.

Slow/frequency flat	Fast/frequency selective
Defocusing	Mulitpath
Effective earth radius and diffraction	

Defocusing/ducting, diffraction and rain fading are usually considered as slow and frequency flat fading events i.e., they usually lasts longer than 10 seconds and affect outage. Multipath fading on the other hand, usually cause fast and frequency selective fading, affecting the short term performance [1]. Multipath fading can last over a few seconds or less. As will be seen, refractive effects are generally dependent on both propagation distance and frequency.

4.2.1 Refractive index

Wave propagation in any media such as air or glass is characterized by the refractive index of the constant defined by

$$n = \frac{c}{v} \tag{4.2}$$

where c is the propagation speed of light in vacuum and v is the propagation speed in the medium. The refractive index of vacuum is therefore given by n=1. There are many phenomenas related to the refractive index and the wave nature of radio signals. Most

known are reflections and refractions which occur on the border between two media with different refractive index. They are explained by the law of reflection given by

$$\theta_1 = \theta_2 \tag{4.3}$$

and law of refraction (Snell's law) given by

$$\frac{n_1}{n_2} = \frac{\sin\theta_2}{\sin\theta_1}. \tag{4.4}$$

In the atmosphere there are in general no distinct borders with media of different refractive index. The atmosphere can be characterized by a smooth gradient of the refractive index under normal conditions as in Fig. 4.3. The refractive index of air is also often approximated to 1, but small changes can have a large impact on radio waves since the propagating distance extend up to hundreds of kilometres.

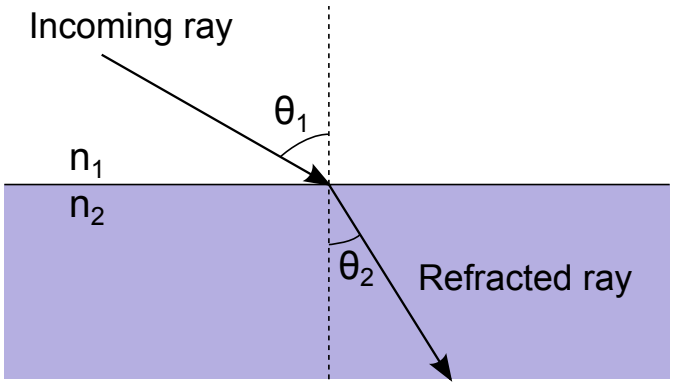

Figure 4.2: Illustration of the law of refraction 4.4. The incoming wave is refracted in border between two media.

In air, the refractive index is mainly affected by parameters such as temperature, humidity and pressure. In the range between 1MHz and 100GHz the refractive index can also be considered independent of frequency [12]. For convenience the modified refractive index, N_{ref} (N-units), is often introduced and defined as

$$N_{\text{ref}} = (n-1) \times 10^{-6}. \tag{4.5}$$

As shown by [12, 13] the refractive index of the atmosphere is given by

$$N_{\text{ref}} = \frac{77}{T}\left(p + 4810\frac{e}{T}\right) \tag{4.6}$$

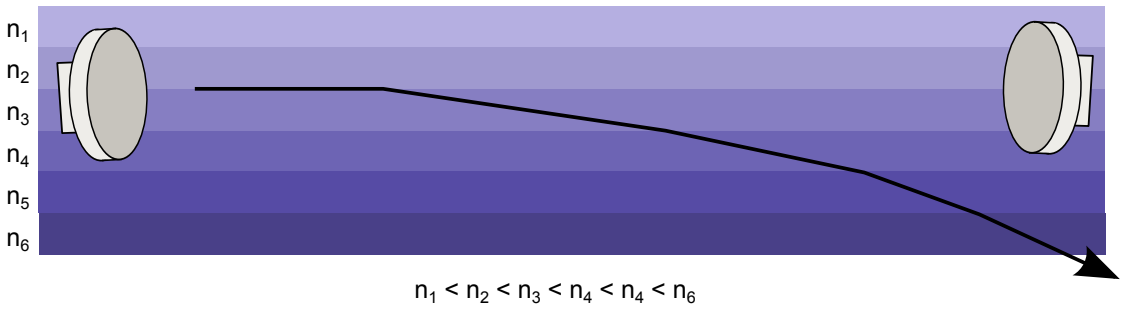

Figure 4.3: A simplified illustration of atmospheric refraction given a gradient of the refractive index.

where T is the temperature in [°C], p is the pressure [hPa] and e is the water vapour pressure [hPa] related to the more commonly used relative humidity [%] as

$$H = \frac{100e}{e_s(t)} \tag{4.7}$$

where e_s [hPa] is the saturation vapor pressure. e_s is derived from empirical equations depending on the temperature, t [°C] according to

$$e_s(t) = a \exp\left(\frac{bt}{t+c}\right) \tag{4.8}$$

where $a = 6.1121$hPa, $b = 17.502$ and $c = 240.97$°C [12]. Based on the formula for refractive index the sensitivity due to variations of temperature, humidity and pressure can be analyzed at different fixed points. The relative change of the refractive index depends on the actual values of the temperature, humidity, pressure etc. Variations are typically largest for humidity and temperature changes. For some typical values, $t = 10$°C, H = 70% and p = 1000 hPa the sensitivities are $dN/dt = 1.43$ N-unit/°C, $dN/dH = 0.57$ N-unit/% and $dN/dp = 0.27$ N-unit/hPa [14]. The most significant change is usually caused by the relative humidity which is known to change rapidly over space and time.

4.2.2 Effective Earth Radius and Diffraction Losses

In the ITU standard conditions for temperate climate, the median refractive index is approximately 315 N-units [12]. The temperature drops about 6 °C/km, pressure with 125 hPa/km and relative humidity is approximately unchanged which gives a refractive gradient of -39N/km. This will cause the radio waves to bend towards the ground [1, 3] and in certain cases, the radio signal can reach beyond the visual horizon.

Another view of the effect of a changing refractive index is given by the concept of effective earth radius. If the refractive gradient is considered constant along the path the effective earth radius means to compensate for the ray-bending. Example, if the rays bends just as much as the real earth curvature the effective earth would look flat for the radio waves, and the effective earth radius would be infinite. The effective earth can be characterized by the so called k_{earth}-factor given by

$$k_{\text{earth}} = \frac{1}{R + \frac{\delta N}{\delta h} 10^{-6}} \tag{4.9}$$

where $k_{\text{earth}} = 1$ represent the actual radius. It is easy to verify that the standard gradient of -39 N-units/km gives the widely used k value of approximately k = 4/3. A refractive gradient of -157 N-units/km gives $k = \pm\infty$. Under such conditions or for smaller gradients the radio signals can travel far beyond the visual horizon with little loss. This is referred as super refractive conditions or ducting. The effective earth radius will be negative which implies that the signal will bend strongly towards the ground. Gradients larger than the normal conditions of -39N/km is referred as sub-refractive conditions. Under such conditions the effective earth radius will appear small and the signal will bend upwards.

The effective earth radius is often used to calculate the needed path clearance of a link. The path clearance is defined as the distance from the geometrical line-of-sight path trajectory to the closest object or the ground. As the effective earth radius decreases the ground or any object will appear higher. This effect is visualized in Fig. 4.4 where the effective ground is shown for three different k_{earth}-values.

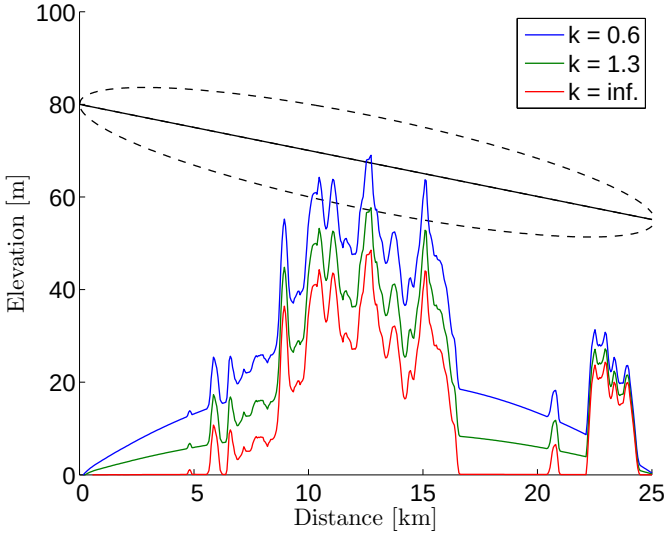

Figure 4.4: Example of effective ground height for some effective earth radius values. The ellipse shows the first Fresnel zone where obstruction losses can be significant.

If the effective ground or any object obstructs the path, it will lead to losses when a part of the signal and energy diffracts around the object. This is called diffraction or obstruction loss. In link design this results in an increased hight clearance requirement, in contrast to the visual line-of-sight. The diffraction loss over average terrain can be approximated for losses greater than about 15 dB as

$$A_d = -20\frac{h}{F_1} + 10[\text{dB}] \tag{4.10}$$

where h is the path clearance [m] between most significant path obstruction and the LOS path trajectory. The height difference becomes negative if the obstruction is above the LOS path. The parameter F_1 is the first Fresnel zone radius which can be calculated from

$$F_k = \sqrt{\frac{k\lambda d_1 d_2}{d_1 + d_2}} \tag{4.11}$$

where F_k is the kth Fresnel zone radius [m], d_1 and d_2 are the distances to both terminals [m] and λ is the wave length [m]. Fresnel zones were first introduced as a method to analyze interference from reflection as later will be explained in Section 4.2.4. However, it can be shown that both diffraction loss and the Fresnel zone radius are dependent on the frequency and can be related to each other [3]. The obstruction is therefore normalized by the Fresnel zone radius.

4.2.3 Ducting

The atmosphere can be seen as a random media where atmospheric properties changes the refractive index over space and time as discussed in the previous section. Normally, the variations are relatively small but large refractive gradient often occurs in combination with formation of air layers with distinct temperature and humidity. Relatively abrupt changes between the layers give rise to very large abnormal gradients of the refractive index which can cause severe bending of the signal. The border region between two air layers with large abnormal gradients can some times trap the signal and therefore effectively act as a wave guide or a duct. For this reason, inversion layer phenomenas are often referred as ducting.

Ducting and inversion refer to a number of effects related to formations of air layers in the lower atmosphere. They can both effect the LOS signal component, induce atmospheric multipath and also cause additional ground scatter because of abnormal propagation that can change the effective reflection points. Air layers most typically form in coastal or tropical regions when moist air from the sea mix with drier inland air. In temperate climate such as central Europe and North America, inversion typically occurs during good weather and clear nights. Inversion in those conditions usually takes place when air

close to the ground cools off quicker than the air above which raises the relative humidity and creates a large negative gradient. Layers can form both close to the ground, creating surface ducts or higher from the ground, creating elevated ducts. Most severe conditions are usually when the duct forms in the same height as line-of-sight. When describing the properties of ducts and the profile of the refractive index, the modified refractivity unit M_{ref} is often used [12]. The M-unit is given from

$$M_{\text{ref}} = N_{\text{ref}} + 157h \tag{4.12}$$

where h is the height over the earth's surface in km. The M-units becomes smaller than the initial value when ducting condition is fulfilled ($dN/dh < -157$ N-units/km). This property makes the measure M_{ref} useful when analysing ducts. Therefore, another practical indicator of ducting events is the so called M-profiles [12, 14]. Fig. 4.5 depicts some examples of typical ducting profiles i.e., elevated and surface ducts. The profiles are given by [14]

$$N(h) = N_0 + G_N h + \frac{dN}{2} \tanh \frac{2.96(h - h_0)}{dh} \tag{4.13}$$

where h is the elevation [m], N_0 is the refractive index [N-unit] at $h = 0$, G_N is the nominal refractive gradient [N-unit/m], h_0 is the elevation of the duct [m], dN is the duct depth [N-units] and dh is the duct width [m].

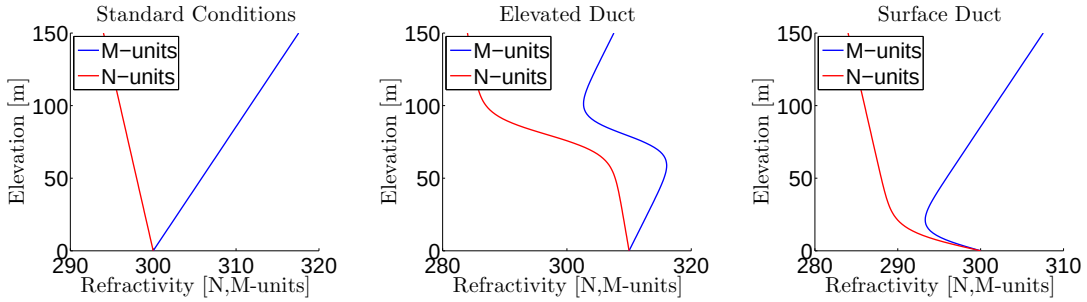

(a) Standard gradient, -39 N-units/km

(b) Elevated duct, $h_0 = 80m, \delta h = 40m, \delta N = -20$

(c) Surface duct $h_0 = 0m, \delta h = 40m, \delta N = -20$

Figure 4.5: Example of two duct profiles and the standard gradient.

Propagation through ducts, inversions or other abnormal change of the refractive index can have an adverse effect on the received signal. In agreement with performance prediction methods [2, 15] and ray-tracing simulations, the effects are enhanced with both hop length and frequency. A longer hops means the signal will likely propagate longer through abnormal refractive media and deviate more from the nominal propagation. This increases probability of focusing and defocusing phenomenas. For multipath the difference in distance between the line-of-sight and the multipath component may also increase, which increases the probability of destructive interference.

The effect of signal propagation through an elevated duct over 10km is simulated with ray-tracing and shown in Fig. 4.6a. In the figure, it seen that the rays of the signal bend little from nominal conditions. The distance axis represents the distance along the Earth's surface, wherefore the rays will appear to bend upwards from the ground. Reflections at Earth's surface have been added to visualize presence of reflections. Fig. 4.6b shows the same scenario over 30km and as seen the ray-bending becomes much more severe. The figures also visualize some typical effects of focusing/defocusing where the rays combine or diverge.

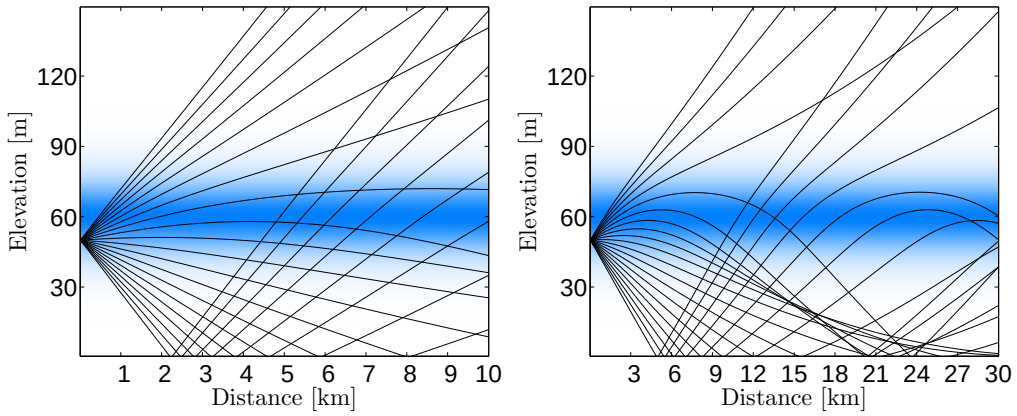

(a) Propagation over 10km. **(b)** Propagation over 30km.

Figure 4.6: Example of two ray tracing simulation through an elevated duct 4.13 with different propagation distance.

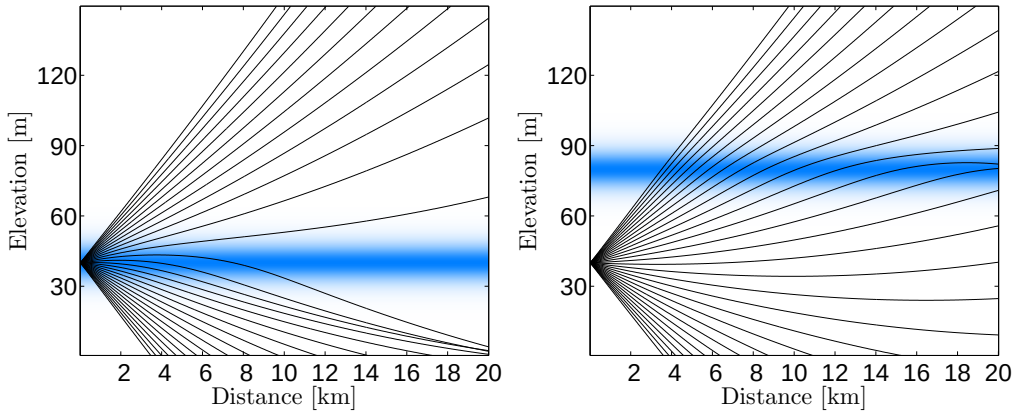

(a) Horizontal propagation **(b)** Inclined propagation

Figure 4.7: Example of a horizontal and inclined propagation through a duct over 20 km.

The effects are frequency dependent, especially when multipath or scatter is present. Higher frequencies usually increase probability of severe fading due to larger phase variations of the multipath components. Another important aspect is the angle of arrival of

the signal through the duct. The impact of the angle of arrival is more severe for small angles. An inclined path will make the signal propagate quickly through the horizontal layer without much effect as is illustrated in Fig. 4.7a. and 4.7b.

4.2.4 Multipath

Both atmospheric multipath and multipath from surface reflections are strongly related to ducting and abnormal propagation. Abnormal propagation can quickly change the delay and distance of a multipath component. Mulitpath fading usually becomes more severe in combination with strong ducting or defocusing events when the LOS component is weaker than nominal conditions. The multipath components can become dominant which lead to a fast frequency selective fading [16, 17]. Multipath or scattered signals are usually not desirable in LOS microwave links. Multipath can arise from strong (specular) reflection from flat surfaces or refractions in the atmosphere. Scattering is usually origins from multiple weak reflections from the ground and surrounding objects.

The received signal is dependent on the relative phase and amplitude between the multipath and LOS component. The farther away the reflection occurs from the LOS path the greater the difference in distance will be between the components. This concept is generalized by Fresnel zones where the reflection on the border between such zones results in constructive (even zones) or destructive (odd zones) interference.

As mentioned earlier, variations of the effective earth radius and the propagation conditions may also change the effective reflection points. Multipath fading can therefore change very quickly, in order of seconds or less [1, 3]. Generally, it is difficult to predict the effect of scatter and non-specular reflections. For MIMO systems it is even harder to foresee the effects due to the several slightly separated MIMO paths as illustrated in Fig. 4.8.

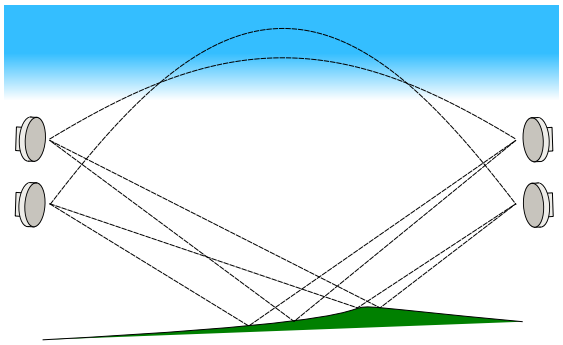

Figure 4.8: Illustration of refraction and reflection in LOS-MIMO system.

4.2.5 Electrical distance

The electrical distance is another important phenomena related to the refractive index of the atmosphere. The electrical distance between two points can be expressed in the duration of travel τ, determined by the propagation speed v in (4.2) or directly in terms of the geometrical distance and refractive index. The electrical distance is given by

$$d_{\text{electrical}} = nd \tag{4.14}$$

where d is the geometrical propagation distance. For microwave frequencies even very small variations of the refractive index can lead to significant phase changes. This effect has been measured by for example [18]. For a LOS-MIMO system, uncorrelated changes of the electrical distance may lead to additional fading and system penalty but it is beyond the scope of this report to study this effect.

5

Channel Models

In this Chapter we will present the ITU method to predict long term variations of a microwave link channel. We will also present analytical channel models motivated by measurements in Chapter 6 to evaluate short term performance.

Many physical phenomenas are known to cause fading and affect performance of a link. The most significant ones were described in the previous section. There are different types of channel models but it is possible to roughly divide them into two classes; physical and analytical models [19]. In addition to channel models there exist several semi-empirical fading prediction methods such as the ITU methods. A prediction method aims to predict the statistical outcome of the channel. A physical model aims to reproduce the actual propagation environment, from geometry to atmospheric conditions. A physical model can often be extensive and complex but also very accurate. Analytical models aim to characterize the impulse response of the channel between each a transmitter and receiver pair. Analytical models often intend to characterize a channel subjected to specific weather conditions. They are therefore useful to analyse systems short term performance. The empirical methods such as the ITU use both analytical models and empirical data over weather and environmental conditions to predict a total fading distribution over the whole year.

For a conventional Single-Input-Single-Output (SISO) link, there exists many channel models and methods to predict variations and statistics of the received power [1]. ITU Rec. P.530 [2] is considered as industry standard and provides a semi-empirical model based on comprehensive measurements. It is good for an initial planning purpose. More detailed models of short term fading have often resulted in analytical and propagation motivated models. Depending on the complexity, these models can provide a more accurate reproduction of real channels [19].

Microwave MIMO channels differ from its SISO counterpart with several slightly spatially

separated paths. Since the separation is small and the signals propagate in common media a high degree of correlation between the signals can be assumed. This is also shown from studies on microwave links with two or more spatially separated receives for diversity protection [2, 20, 21]. Some available studies have investigated amplitude correlation for severe fading events but little is known about phase and amplitude correlations for any fade depth. The phase correlations are important because it can change the orthogonality condition (3.9) of the channel and therefore increase the system penalty.

An important property of most microwave models is that the received power at deep fades ($\gtrsim$ 10dB) is assumed to follows Rayleigh statistics during refractive fading. This gives rise to a characteristic Rayleigh slope of 10dB-per-decade of the deep fade probabilities. This property has been extensively verified by measurements. Meanwhile, more shallow fades are often assumed to be log-normal or as in the case of the ITU-model follow an empirical distribution [3, 22, 23, 24].

In the following sections the ITU prediction methods will be described together with some common analytical models applied on microwave links. Their properties, advantages and disadvantages will be explained. Later equivalent MIMO channel models will be described.

5.1 Path-loss

Path-loss is the reduction of power density of an electromagnetic wave that propagates through space. The loss is proportional to the propagation distance and is present to to any wireless communication system. Path-loss is one of the major components when analysing the link budget. For the case of LOS propagation through a homogeneous media and full clearance of the first Fresnel zone, the path-loss L is approximated with the free-space loss calculated with Friis formula (5.1)

$$L = 20 \log_{10} \left(\frac{4\pi d}{\lambda} \right) \tag{5.1}$$

where d is the propagation distance and λ is the wave-length. The formula is derived from the expansion of a spherical wave when $d \gg \lambda$ e.g. far field condition.

5.2 ITU Method

The ITU method is often considered an industry standard of availability prediction methods [1]. The model considers both rain and refractive fading. It also discusses some key design parameters as antenna height and clearance to reduce outage due to diffraction. The model is semi-empirical in the sense it heavily relies on measurements to fit the models. Rain end refractive fading are considered independent event by the ITU

method, which is divided to handle rain fading, refractive fading and frequency selective distortion separately. Multipath caused by refractive fading is generally considered to fast varying ($< 10s$) and affect performance while rain is slow varying ($> 10s$) and affects outage.

5.2.1 Rain Attenuation

The specific rain attenuation is described in section 4.1. The total rain attenuation of the link is given by the hop length and the specific attenuation for a specific rain rate. Statistical data for rain rates are often readily available which makes it straight forward to predict attenuation caused by rain. However, the rain rate may vary along the hop and the ITU method compensates for this effect by calculating an effective rain distance factor, r_{eff} given by

$$r_{\text{eff}} = \frac{1}{0.477 d^{0.633} R_{0.01}^{0.073\alpha} f^{0.123} - 10.159(1 - e^{-0.024d})} \tag{5.2}$$

where $R_{0.01}$ is the rain rate exceeded 0.01% of the year and α is the same coefficient as from (4.1). The rain rate $R_{0.01}$ together with the distance d and the effective rain distance factor r_{eff} is used to calculate the rain attenuation exceeded 0.01% of the year,

$$A_{0.01} = \gamma_{\text{R}} d r_{\text{eff}} \tag{5.3}$$

where γ_{R} is the specific rain attenuation given for the rain rate exceeded 0.01% of the year. The full method also provide formulas for other percentages of time [2].

5.2.2 Refractive fading

Refractive fading is known to be caused by many propagation effects but ITU provide a method to calculate the total distribution of the fading. Multipath fading is believed to cause the 10dB-per-decade slope of the distribution, often under influence of other effects such as defocusing [2, 16]. Here, the channel is assumed to be narrow-band and the fading to be frequency-flat. Outage due to frequency selective fading are highly dependent on the specific receiver and is thereby handled separately by the ITU method. The ITU method assumes deep fades for a small percentage of time where the amplitude distribution can be characterized by the Rayleigh distribution. The small percentage of time p_w that fade depth A [dB] is exceeded in the average worst month can be calculated from:

$$p_w(A) = p_0 \times 10^{(-A/10)}[\%] \tag{5.4}$$

where p_0 is called multipath occurrence factor i.e., the distribution interpolated to $A = 0$. The multipath occurrence factor p_0 depends on hop length, frequency, weather and terrain characteristics. It can be measured, or calculated as

$$p_0 = Kd^{3.1}(1 + |\epsilon_p|)^{-1.29} f^{0.8} \times 10^{-0.00089 h_L} [\%] \tag{5.5}$$

where K is the geoclimatic factor, d is the path length (km), ϵ_p is the path inclination, f is the frequency (GHz). The path inclination is given by $|\epsilon_p| = (|h_t - h_r|)/d$, where h_t is the height of the transmitter (m) and h_r of is that of the receiver. The geoclimatic factor K is a key parameter for the inherent properties of the terrain and the climate of the current location. Different estimation methods exist if measurement data is not available [2]. For quick calculation of K , one can use:

$$K = 10^{-4.6 - 0.0027 \mathrm{dN}_1} \tag{5.6}$$

where dN_1 is the point refracted gradient in the lowest 65m of the troposphere that is not exceeded for more than 1% of the year. The value can be obtained from measured data or acquired from ITU [12].

The distribution for a small percentage of time can be extended to all percentage of time and any fade depth by an empirical interpolation [2]. The method is described in detail in [2]. The full distribution of fade depths for several values of p_0 is given by Fig. 5.1. Notable is the 10dB-per-decade slope of the probability of exceeded fade depths. Increased p_0 increases the probability of deep fades.

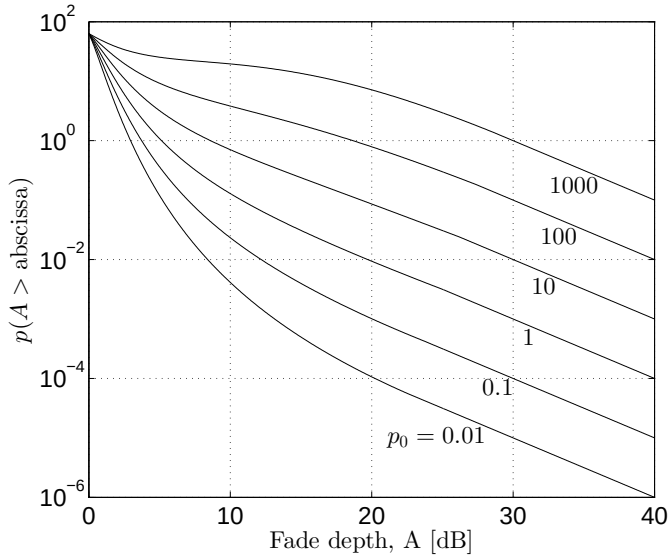

Figure 5.1: ITU fade depth distribution of refractive fading for different values of the multipath occurrence factor, p_0. [2]

5.2.3 Outage Due to Distortion

The main cause of signal distortion include multipath propagation that causes frequency-dependent, amplitude and phase variation [2, 22]. In digital systems such distortion is handled by different types of equalizers. If the distortion itself generates an outage, it might not help by increasing the fade margin. In this case, the ITU model predicts the outage of such distortion using a so called signature method, where the systems ability to handle in-band distortion is derived [2]. Currently, there is no equivalent signature method for MIMO systems since the path correlation of the MIMO channel is not known. However, some simulations on specific cases of frequency selective channels have been performed by [9].

5.3 Analytical Models

A common analytical model describing SISO systems is the multi-ray model where the channel is characterized by the statistics of each multipath components. However, MIMO channels are often described by multivariate distribution to capture correlated fading between the MIMO paths. In this section, an extension of the multi-ray model is proposed to cover the MIMO case by describing each channel component using multivariate random variable.

5.3.1 Multiple-path Models

The fading during refractive fading has often been found to be composed of several components [22, 23, 24, 25]. In particular the channel often contains a frequency-flat component from defocusing and other slow-varying effects, and also a fast-varying, frequency-selective component mainly caused by ground scatter [3, 16, 17]. Based on the above observation, a propagation motivated multi-path model has been proposed given by

$$h = \sum_i a_i e^{\left(j\frac{2\pi}{\lambda}\tau_i\right)}. \tag{5.7}$$

The multi-path model produces the channels impulse response for a limited time. Hence it does not provide any outage prediction for all the time but it is useful to in detail study the performance of a systems under specific fading events. If needed, the probability of fading events can then be used to calculate the overall outage. In an extension of the multi-path model to cover MIMO cases, the single path component will be replaced by the MIMO channel component $\mathbf{H}_i$. Each multipath MIMO channel represents a reflection or scatter from the same area. For wide-band channel it is assumed that every element of the MIMO multipath component has the same delay, τ_i as (5.8)

$$\mathbf{H}(f) = \sum_i \mathbf{H}_i e^{(j2\pi f\tau)} \tag{5.8}$$

when the separation between the antennas is relatively small. However in this report we have focused on narrow-band systems where the delay is approximately zero.

5.3.2 Correlated Rician and Rayleigh Model

A very common analytical model in literature for LOS-propagation is the Rician channel [6, 19]. From our real-world measurements presented in Chapter 6 the Rician model works also well to model multipath fading. In this context the Rician channel can be seen as a special case of the general two-ray model used to model fast-varying effects. The Rician channel is given by

$$\mathbf{H} = \sqrt{\frac{\kappa}{1+\kappa}}\mathbf{H}_{\text{LOS}} + \sqrt{\frac{1}{1+\kappa}}\mathbf{H}_{\text{NLOS}} \tag{5.9}$$

where κ is the Rician factor, $\mathbf{H}_{\text{LOS}}$ is the $N \times N$ normalized deterministic channel. As a result of small spatial separation between antennas, the elements of the NLOS $N \times N$ channel component, $\mathbf{H}_{\text{NLOS}}$, are assumed to be correlated Gaussian distributed with equal mean and variance. A special case of the Rician channel with no significant static deterministic component is the Rayleigh channel given by

$$\mathbf{H} = \mathbf{H}_{\text{NLOS}}. \tag{5.10}$$

The distribution of $\mathbf{H}_{\text{NLOS}}$ is given by [19, 26]

$$p(\mathbf{h}_{\text{NLOS}}) = \frac{1}{\pi^{N^2}\det(\Sigma_{\text{NLOS}})}\exp\left(-\mathbf{h}^*_{\text{NLOS}}\Sigma^{-1}_{\text{NLOS}}\mathbf{h}_{\text{NLOS}}\right) \tag{5.11}$$

where $\mathbf{h}_{\text{NLOS}} = \text{vec}\,(\mathbf{H}_{\text{NLOS}})$ and $\text{vec}\,(\cdot)$ is the vectorization operator, Σ_{NLOS} is the covariance matrix. Σ_{NLOS} contains information of the correlation structure between the paths. To be able to study MIMO path correlation, we define a simple correlation structure and the correlation matrix to be

$$\Sigma_{\text{NLOS}} = \mathbb{E}[\mathbf{h}_{\text{NLOS}}\mathbf{h}^*_{\text{NLOS}}] = \begin{bmatrix} 1 & \rho_{21} & \cdots & \rho_{N^2 1} \\ \rho_{12} & 1 & & \\ \vdots & & \ddots & \\ \rho_{1N^2} & & & 1 \end{bmatrix} \tag{5.12}$$

where all elements have equal correlation magnitude but correlation phases are specified by the LOS channel $\mathbf{H}_{\mathrm{LOS}}$. This is motivated by the small spatial separation of the MIMO paths. Hence, the absolute values of the elements of Σ_{NLOS} are given by $|\rho_{ij}| = \rho$ where $|\cdot|$ is the absolute value. The correlation phases are given by $\angle\rho_{ij} = \angle h_{\mathrm{LOS},i} - \angle h_{\mathrm{LOS},j}$ $\forall i \neq j$, $|\rho_{ii}| = 1$ and $\angle\rho_{ii} = 0$ where $\arg(\cdot)$ is the argument function. The element $h_{\mathrm{LOS},i}$ is the ith element of the vector $\mathbf{h}_{\mathrm{LOS}} = \mathrm{vec}\,(\mathbf{H}_{\mathrm{LOS}})$ and $i,j \in [1,N^2]$ A lower value of ρ leads to lower correlation between different paths in both phase and amplitude.

It has been shown by many studies that in severe events of refractive/multipath fading the channel can be characterized by Rayleigh fading. From our measurements presented in Chapter 6 and earlier studies [19] we have seen that the Rician channel can be used to model multipath fading. For this reason the Rayleigh and the Rician channel will be used in Chapter 7 later to analyse deep fading distributions and impact of path correlation.

6

Measurements

In order to demonstrate a working LOS-MIMO system and to collect fading data, two microwave 2×2 LOS-MIMO test links were deployed at Ericsson's site in Mölndal, Sweden. The channel fading data were collected to help understand and characterize both long and short term fading in a LOS-MIMO system.

Measurements from the systems were collected during 2012 and until June 2014. A summary of the two links is listed in Tab. 6.1. The first link L1 is 5.3km long and it operates at 8GHz, with horizontally separated antennas. The second link L2 is 1.3km long, and it operates at 32GHz, with vertical antenna separation. An overview of the geographical deployment is shown in Fig. 6.1. Both links are deployed close to optimal conditions according to (3.14) and both links have full clearance and no obstruction within the first Fresnel zone. According to the ITU model the propagation can therefore be approximated with free-space propagation. For the test links, the following parameters were measured and logged to characterize the channel fading to study atmospheric impact:

(i) Received power, P_{RX}
(ii) MIMO phase $\Delta\theta$ (3.15)

In addition, meteorological data, such as wind speed, temperature, humidity, pressure and rain rate was measured at two 15m vertically separated weather stations at Ericsson's site. Apart from weather conditions these parameters can be used to calculate the refractive index of the atmosphere with (4.6) in Chapter 4. Two measuring points can not give a full picture of refractivity along the entire signal path. However, the measurements from the two weather stations provide us with a useful estimation of the vertical variation of refractivity.

Table 6.1: Link Setup Summary. $(\cdot)$ represent value for the second direction.

Link	Sisjo link	Sahlins link
Label	L1	L2
Location 1	Ericsson	Ericsson
Location 2	Sisjon water tower	Sahlins Terass building
Hop length (km)	5.314	1.355
Frequency (GHz)	7.989 (8.299)	31.815 (32.627)
Antenna separation	Horizontal	Vertical
Polarization	Horizontal	Vertical
Deployment number, η	1.003 (1.022)	0.989 (1.002)

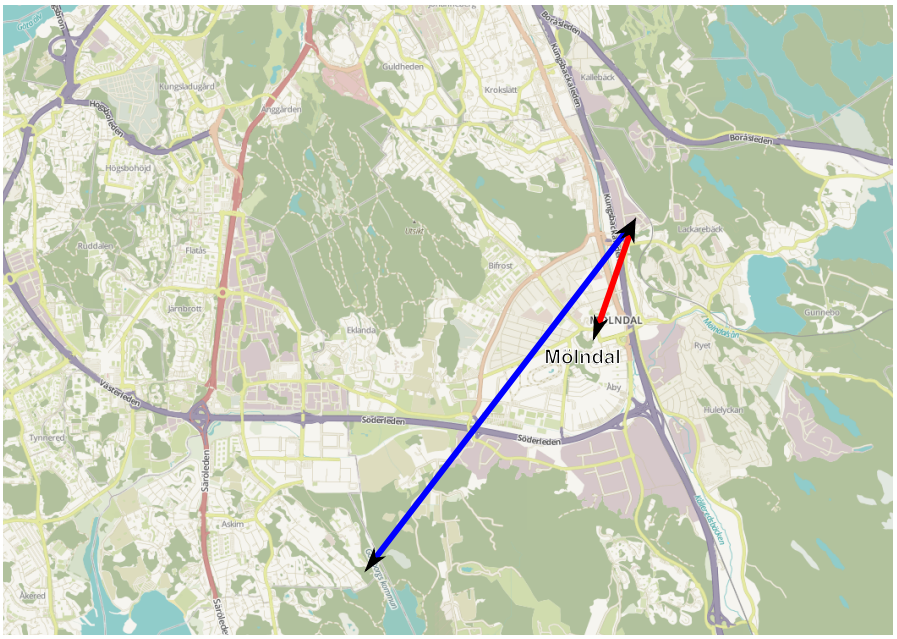

Figure 6.1: Overview of the the geographical link deployment. L1 is represented by the blue arrow and L2 by the red arrow.

6.1 System Structure

The receivers used in the LOS-MIMO test links can be described as a correlation based interference cancelling receivers. A simplified receiver structure is presented by the block digram in Fig. 6.2. At the transmitter, two independent signal streams are transmitted by the two spatially separated antennas. The received signals are sampled and thereafter fed to an equalizer. RX_1 and RX_2 represent the received signal at the two receiving

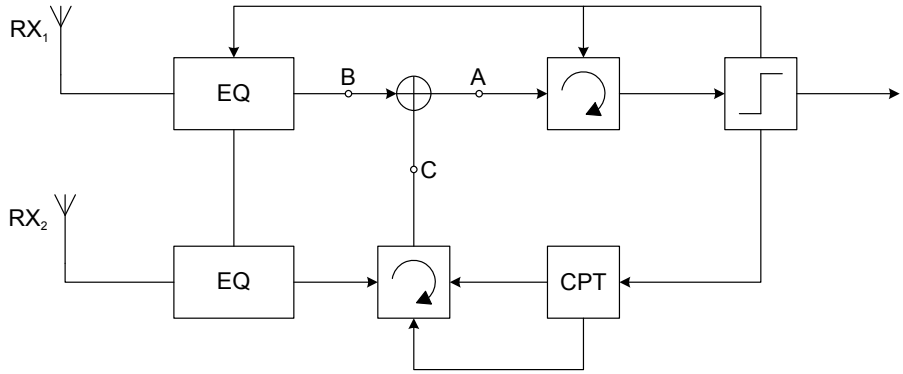

Figure 6.2: Receiver cancellation structure of the prototype receiver. The CPT block represent the Carrier Phase Tracker

antennas in Fig. 6.2. The received signal at RX_1 and RX_2 then consist of a sum of the two transmitted signal streams. From the geometry of the deployment the received signal streams are received at the antennas with independent phases. The received signals are then scaled and rotated so the unwanted interference signal of RX_1 and RX_2 have equal power and are shifted by 180°, and therefore cancel each other out. The signal after cancellation will consist of the sum of the wanted signal stream from RX_1 and RX_2. The process is visualized in Fig. 6.3.

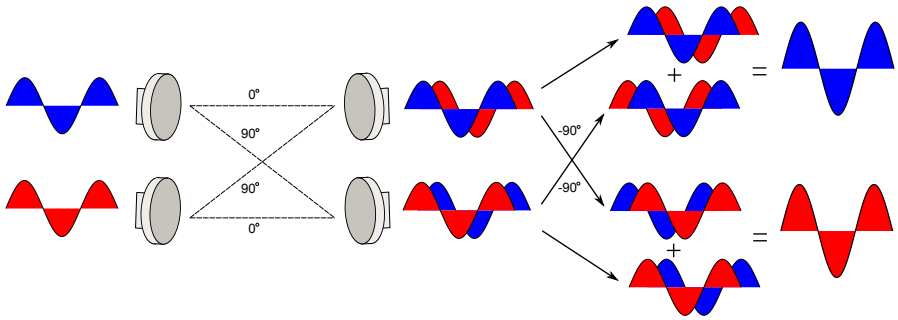

Figure 6.3: Simple illustration of the signal cancellation process.

If the deployment optimality condition are met the wanted signal will have the same relative phase and add constructively. The system will work even if the optimality condition does not hold. In such case, the wanted signal will not have the same phase and therefore the combining cannot be optimal. Finally, the combined signal is rotated and fed to the slicer. Simplified, the system is equivalent to the theoretical ZF-MIMO receiver described in Section 3.1.2.

Two different methods to measure the MIMO phase are used. The first method is a correlation based method used in the LOS-MIMO test links receivers described previously. It is referred as the correlation method. The second method uses the relative phase difference between two sinusoid tones. The method is referred to as the sinusoid

method. The methods are further decried in [27].

6.2 Rain Fading

Rain fading is usually considered an attenuation of the signal power and the path correlation distance likely to be much larger than the antenna separation, therefore rain fading on the MIMO paths is expected to be highly correlated. However from Section 4.1 we know that some studies reports of increased scatter during rain [4, 11]. Even though L1 is longer, L2 is expected to experience more attenuation during rain due to the higher frequency used.

Fig. 6.4a and 6.4b show the received power P_{RX} and the MIMO phase $\Delta\theta$ for L1 and L2 during a typical event of heavy rain over two days in 2013. As expected L2 operating at 32 GHz is much more attenuated during rain than the longer L1 operating at 8 GHz. It was also noted that all four MIMO paths are attenuated almost equally by rain, for the both links. As seen in Fig. 6.4b the MIMO phase does not deviate more during rain than under normal conditions.

Motivated by above observations, the highly correlated rain fading will be modelled as a scalar attenuation of the signal. This suggests that rain affects both MIMO and SISO links with an equivalent penalty. Methods to predict rain penalty should therefore be accurate for LOS-MIMO systems as well.

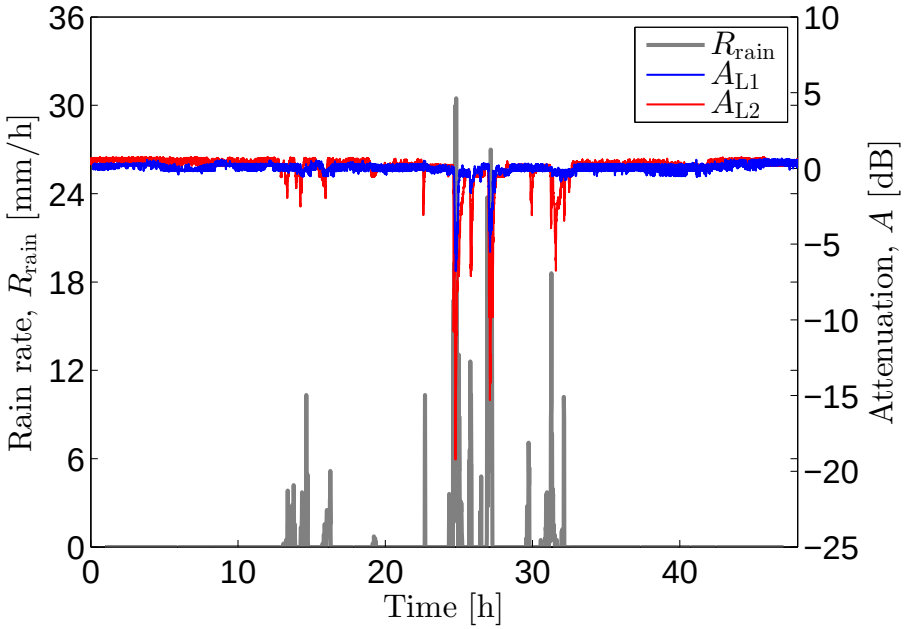

(a) Received power attenuation A

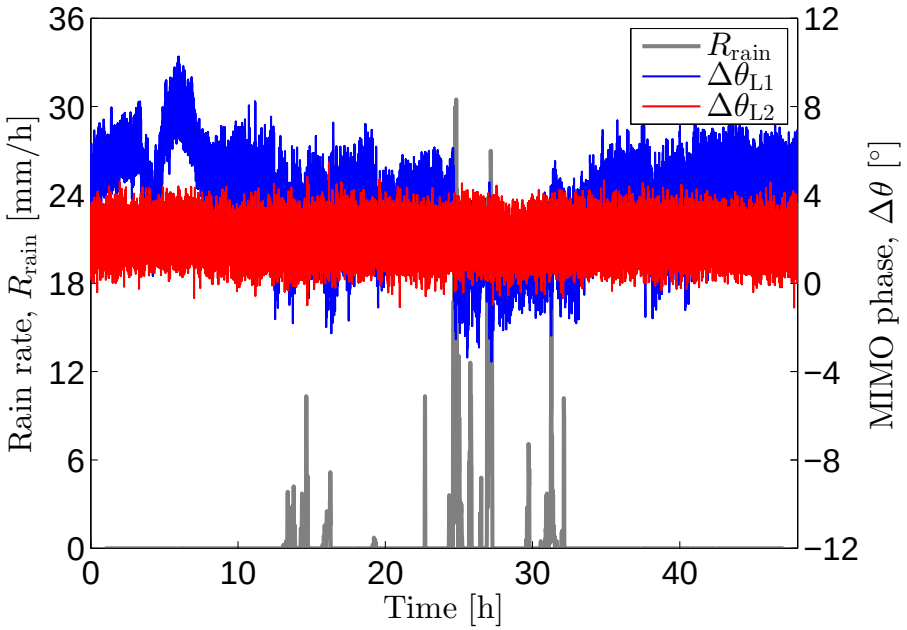

(b) MIMO phase $\Delta\theta$

Figure 6.4: Example of received power attenuation A and MIMO phase measurement $\Delta\theta$ during rain. L1 represent the 5.3km link operating around 8GHz while L1 represent the 1.3km link operating around 32GHz.

6.3 Refractive Fading

From Chapter 4 we know that typical conditions of refractive fading in temperate climate are during windless summer nights. The temperature close to the ground drops quicker than in the air above which causes the formation of air-layers with distinct refractive properties. Variations of the refractive properties cause abnormal propagation phenomena such as ray-bending, defocusing/focusing and multipath propagation. Fig. 6.5 shows temperature and wind speed for a characteristic event of refractive fading for two days in 2013. The temperature drops during night and the wind speed approaches zero.

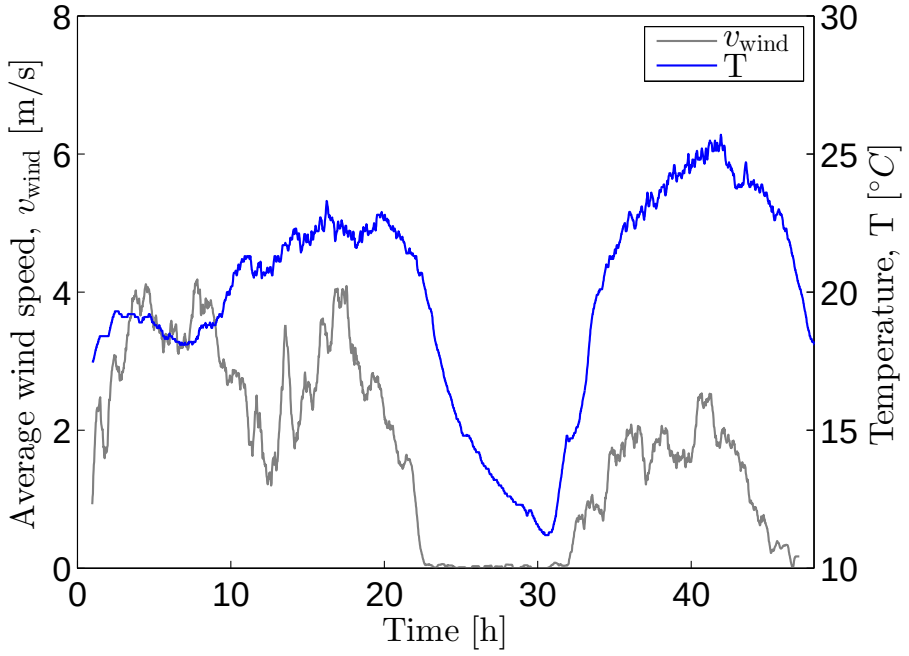

Figure 6.5: Temperature and wind speed during 48h. The conditions are typical for formations of air-layers and refractive fading.

Fig. 6.6a and 6.6b show the variations P_{RX} and $\Delta\theta$ during the typical event of refractive fading. Relatively large variations of both P_{RX} and $\Delta\theta$ were observed on L1 during the night when the temperature dropped and the wind speed was low. This indicates multipath fading caused by abnormal refractive conditions. From (5.5) it follows that multipath activity is largely proportional to the hop length $\propto d^{3.1}$ which can explain why L1 experienced more fading than L2.

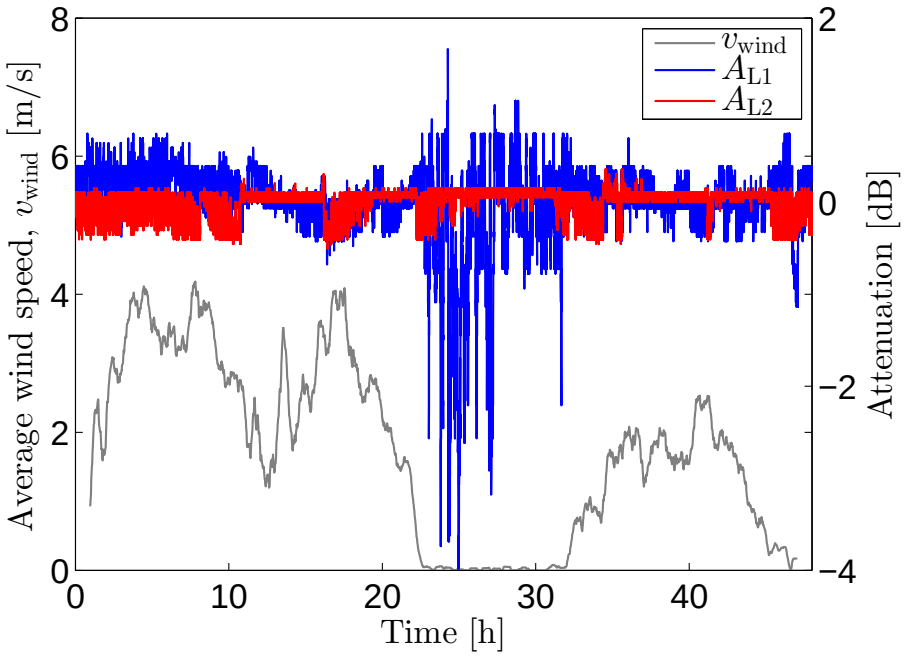

(a) Received power attenuation

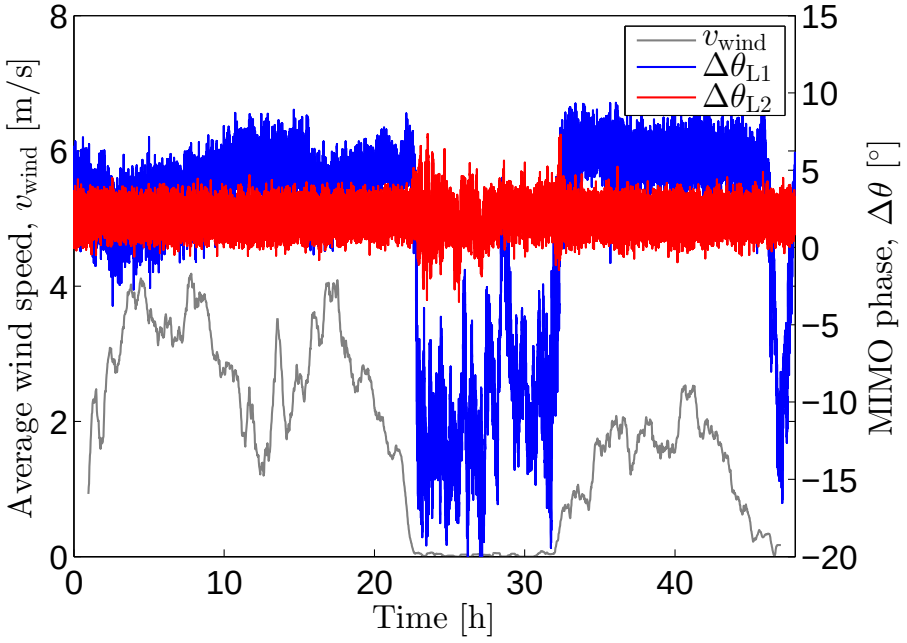

(b) MIMO phase $\Delta\phi$

Figure 6.6: Received power and MIMO phase measurement during a typical event of refractive fading. L1 represent the 5.3km link operating around 8GHz while L1 represent the 1.3km link operating around 32GHz.

It is shown from the previous example that increased refractive fading is observed between 22h to 32h. The cumulative distribution function CDF of P_{RX}, ΔP and $\Delta\theta$ during these hours for L1 is plotted in Fig. 6.7. In the same figure, we also depict the Rician model (5.9) which fits well with the measurement data. The good agreement indicates that the Rician model is a useful model during refractive fading. The Rician factor during the specific event was determined to $\kappa = 16$ dB, the correlation to $\rho = 0.93$ and the correlation phases according to the geometrical deployment. It is noted that the correlation is high and the variations are small compared to studies on other links [20, 22, 24, 28].

MIMO C/I (Carrier-to-Interference ratio), ΔP, is for the 2×2 MIMO system defined by (6.1)

$$\Delta P = \frac{|h_{11}|}{|h_{12}|}\frac{|h_{21}|}{|h_{22}|} \tag{6.1}$$

was introduced for the distribution plots as it showed to be a practical measure to study correlations of amplitude variation of the MIMO paths. Correlated fading will leave the MIMO C/I unchanged and a pure LOS channel will result in $\Delta P = 1$ if all antennas have equal gain.

6.4 MIMO Phase and Deployment

To verify the deployment penalty and the MIMO phase $\Delta\theta$ measuring methods, $\Delta\theta$ was measured with both the correlation method and the sinusoid method [27]. The test were carried out by an initial antenna separation that was smaller than optimal. The antenna separation was then increased in small steps for which $\Delta\theta$ were measured . For comparison $\Delta\theta$ was also calculated from the geometrical path lengths. The result is shown in Fig. 6.8. A similar plot for the calculated and measured penalties are shown in Fig. 6.9.

It is seen in the figures that both the correlation and the sinusoid method show fairly good agreement with the geometrical calculation. The deviation of the measured and the calculated values is possible due to approximation of free-space conditions for the geometrical calculations or hardware impairments.

6.5 Worst Month Measurements

In this section we present long term measurement for refractive and rain fading during the worst month. Worst month is studied because fading is not equally distributed over the year. Worst month distribution is also considered by the ITU methods. Fig. 6.10a and 6.10b shows the worst month (July-August 2013) system penalty distribution for

L1 and L2. It is shown that rain have the most substantial impact on the fading on the measured fading distribution. For L1, the ITU method for refractive fading clearly overestimate the fading impact. This can partly depend on the relative short hop-length and that the distribution is estimated in the shallow fading region $\lesssim 10$. It is noted that the system penalty and the received power distribution during the worst month was nearly identical and therefore not represented by separates graphs. This can be explained by highly correlated fading, small MIMO phase variations and that, in this case, rain is the dominant source of the fading. On other links there can be a difference in distribution between received power and system penalty as will be analysed in Chapter 7.

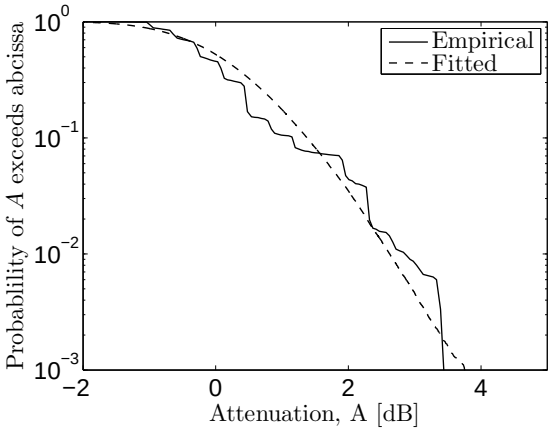

(a) Received power CDF refractive fading

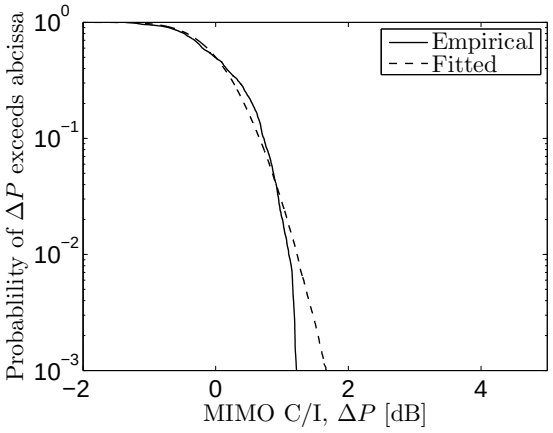

(b) MIMO C/I CDF during refractive fading

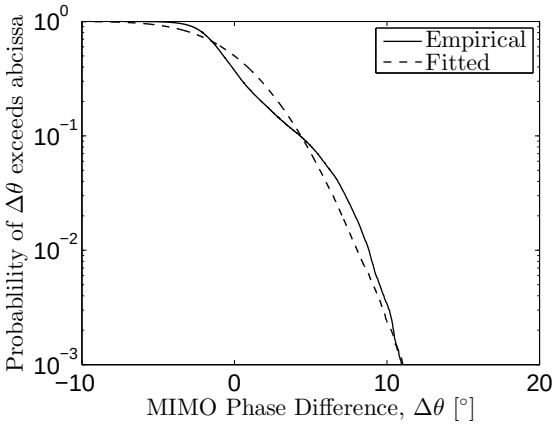

(c) MIMO phase *cdf* refractive fading

Figure 6.7: The cumulative distribution function CDF of P_{RX}, ΔP and $\Delta\theta$ between 22h and 32h during the refractive fading event on L1. Fitted with a Rician channel (5.9) with $\kappa = 16$dB and $\rho = 0.93$.

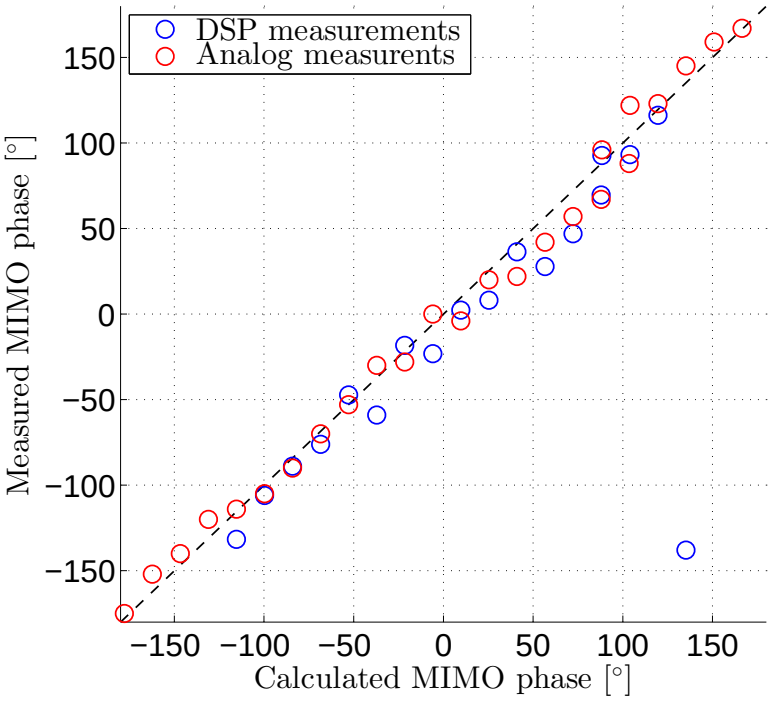

Figure 6.8: Comparison between measured and calculated MIMO phase $\Delta\theta$ from deployment.

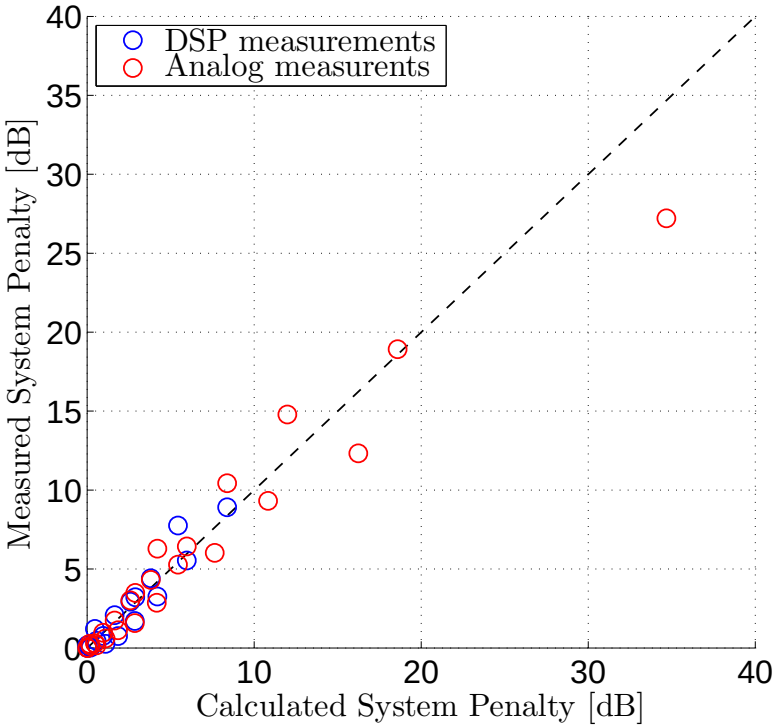

Figure 6.9: Comparison between measured and calculated system penalty γ from deployment.

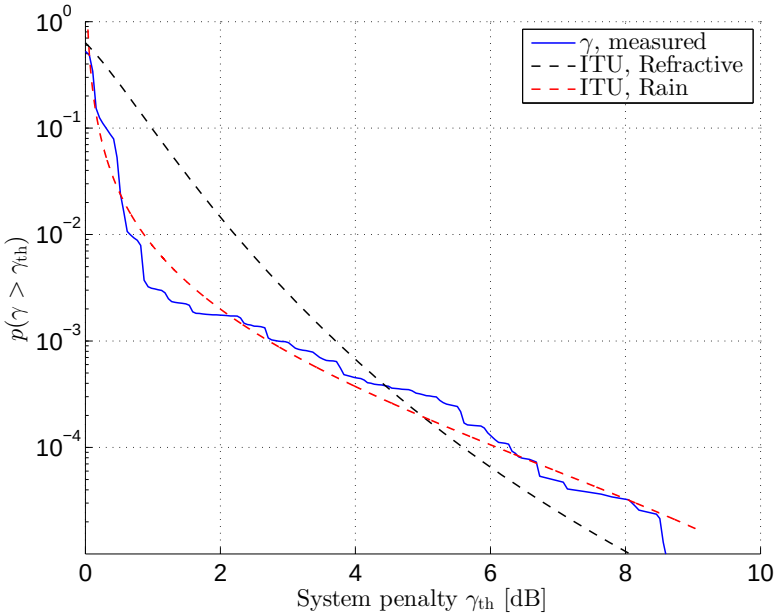

(a) System penalty on L1.

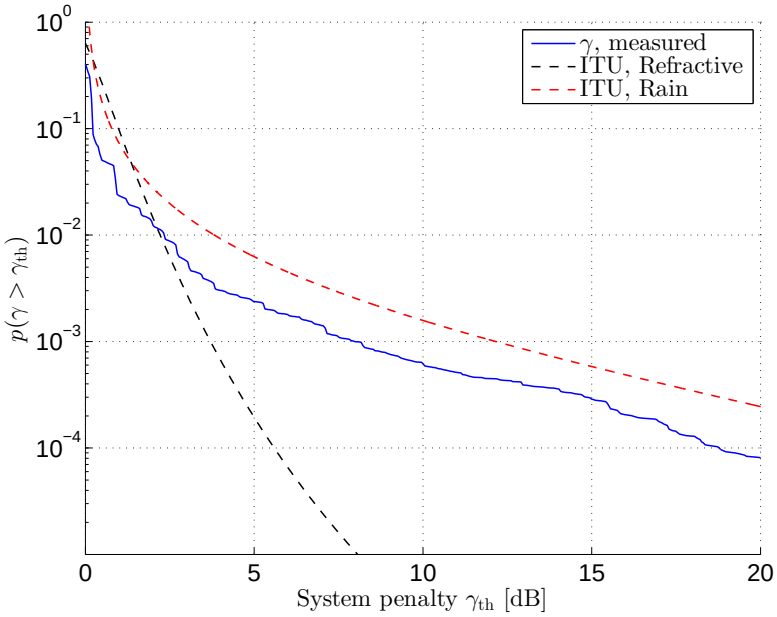

(b) System penalty on L2.

Figure 6.10: Worst month CDF of measured system penalty on L1 and L2. ITU predicted fading distributions are added for comparison.

7

Analysis

In this section, we present an analysis of the performance of a narrow-band system given a Rician channel model (5.9). This analysis can help us to gain understanding of the performance of MIMO systems during refractive fading. In particular, we are mainly interested in the deep fading region with the multipath characteristic 10dB-per-decade slope of the fade depth. As availability is one of the key factors for microwave links and high power margins are usually employed, outages most typically occur in this fading region [1]. The 10dB-per-decade slope characteristic is well-documented for real-world SISO links and therefore it is interesting to investigate if MIMO system penalty distribution have similar properties, and if SISO and MIMO system penalties can be related to each other.

We will present some numerical simulations to demonstrate the effect of multipath activity and the significance of correlation of MIMO paths given Rician or Rayleigh channels. In particular, we consider a 2×2 ZF-MIMO and a 2×2 SVD-MIMO system with optimal deployment ($\eta = 1$), thus $\mathbf{H}_{\mathrm{LOS}}$ from (5.9) will have full rank. Later we will investigate the penalty distribution in terms of sub-optimal deployment.

7.1 Multipath Activity

In this section we present simulations of the impact of multipath activity (multipath fading). In this scope the multipath fading represent fading during abnormal refractive conditions according to [2] and measurements in Section 6.3. In simulations we first consider a ZF-MIMO system in a Rician channel (5.9) for a changing value of the Rician factor κ. Generally in microwave links, multipath fading is often associated with reduction of the overall received power of the signal, but to narrow down on the multipath

effect we use a normalized channel.

First, in Fig. 7.1, the ergodic capacity (3.18) for a Rician channel is plotted against κ for different values of the correlation coefficient ρ in (5.12). It is seen that the capacity decreases slightly as κ decreases. Fig. 7.2 shows the outage probability, given penalty margin of 20dB, against κ. It shows that decreased κ leads to a larger probability of outage. It is also observed that decreased correlation, ρ, leads to a reduction of capacity and increased probability of outage. The changes can be related to the channel optimality condition in (3.9) ,e.g., decreased ρ leads to larger variations of the MIMO phase $\Delta\theta$ and also variations of the system penalty γ_{ZF}. In total it is noted that decreased κ leads to a relatively small ergodic capacity loss. A more significant impact is the increased outage probability which we will see is related to the distribution of the system penalty. In microwave links this implies that increased multipath activity leads to increased outage probability even though the average signal level also need to be considered for real links.

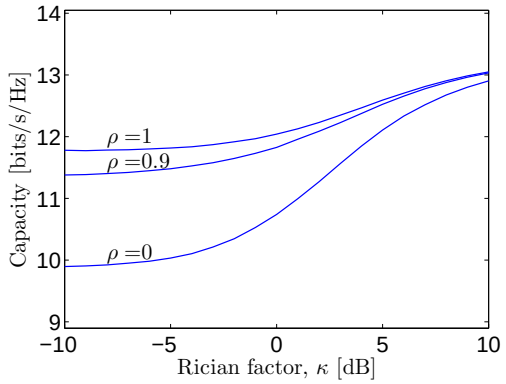

Figure 7.1: The ergodic ZF-MIMO capacity against the Rician factor κ for several correlation coefficient ρ. SNR=20dB.

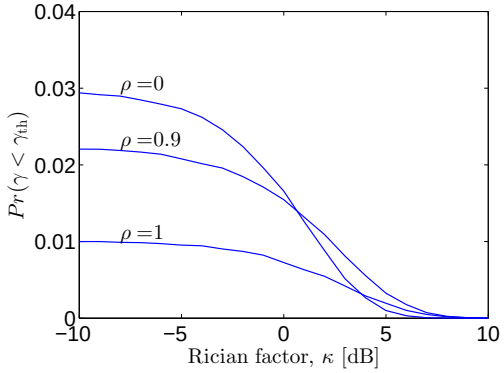

Figure 7.2: Outage probability against the Rician factor κ for several correlation coefficient ρ and $\gamma_{\mathrm{th}} =$ 20dB.

7.2 Penalty Distributions

In order to provide some insights at how fading affects the performance and outage of a LOS-MIMO system we will have a closer look into penalty distributions. A key focus will be to compare MIMO with SISO systems. In particular, the penalty distribution of the three receivers below will be compared:

(i) ZF-MIMO system
(ii) SVD-MIMO system
(iii) SISO system

The penalty for a SISO system γ_{SISO} is equivalent to a single path attenuation. Accordingly, if $\rho = 1$ the fading can be seen as a scalar factor wherefore all four systems will have equal penalty distribution. We first look at the system penalty γ distribution in the Rician channel with $\rho = 1$ for some values of κ in Fig. 7.3. It is seen that the tails of the distributions follow the 10dB-per-decade slope for various values of κ which suggests that Rician channels can model this 10dB-per-decade characteristic.

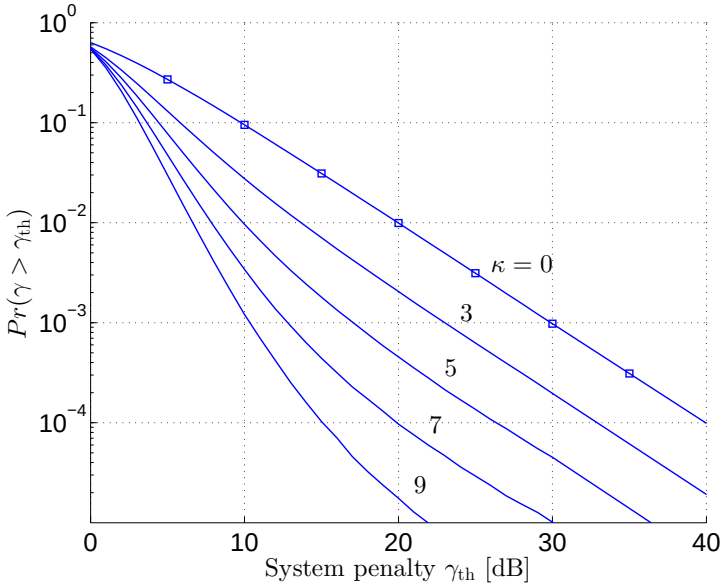

Figure 7.3: System penalty CCDF for all systems in a fully correlated Rician channel given $\rho = 1$ for some values of κ.

To gain insight into how the correlation coefficient ρ affects the penalty distributions we conducted simulations in Fig. 7.4 and Fig. 7.5. In Fig. 7.4 we consider a correlated Rayleigh channel (5.10) as a typical worst case of multipath fading. In earlier studies the Rayleigh channel has often been used to model severe refractive fading for microwave links [20, 22, 28].

The complementary cumulative distribution function (CCDF) of the penalty for the 2×2 ZF-MIMO receiver in the Rayleigh channel is shown in Fig. 7.4a for various values of ρ. The distribution of γ_{SISO} is included for comparison and it remains equal to γ_{ZF} given $\rho = 1$. Simulations show that the distribution γ_{ZF} is moderately affected by ρ. The slope of the distribution tails follows a 10dB-per-decade slope, equivalent to γ_{SISO}. Reduced path correlation corresponds to an additional penalty. Next, the penalty distribution of an SVD-MIMO receiver is plotted in Fig. 7.4b. It is seen that the SVD-MIMO receiver performs similarly to or better than the SISO receiver in terms of outage. Especially, the improvement becomes more significant as the correlation coefficient ρ decreases, which can be explained by reduced probability of large penalties.

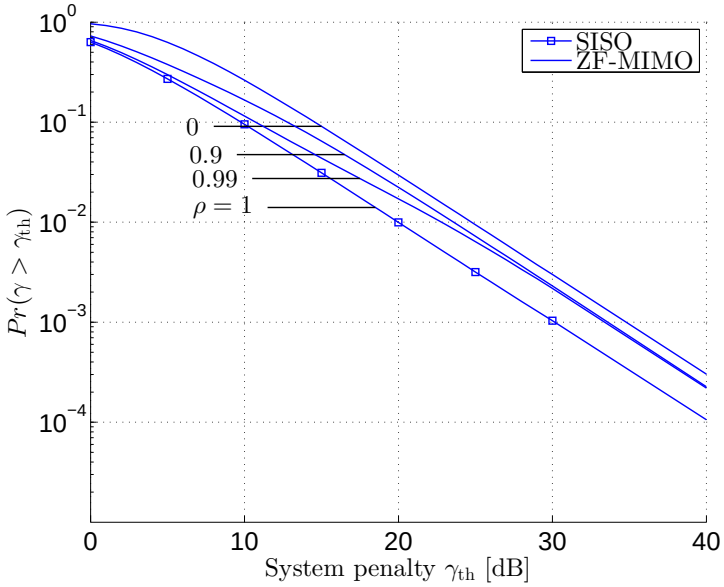

(a) System penalty CCDF for ZF-MIMO system.

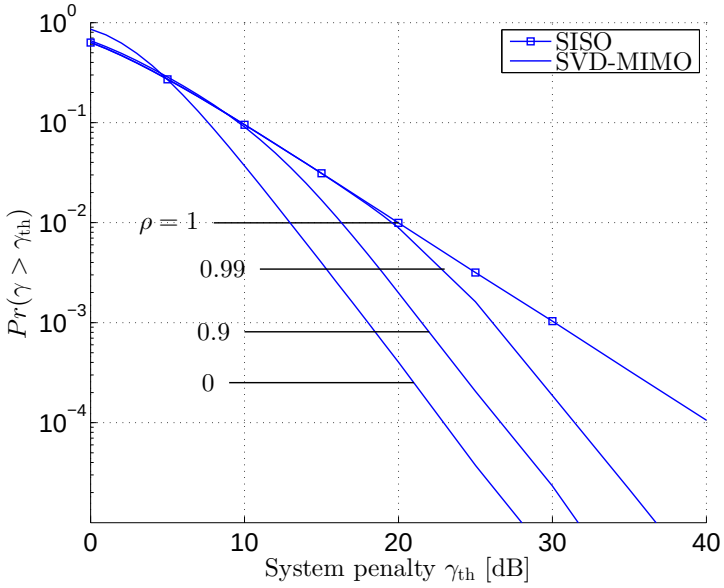

(b) System penalty CDF for SVD-MIMO system.

Figure 7.4: System penalty CCDF for ZF-MIMO and SVD-MIMO systems in correlated Rayleigh channel for several values of ρ.

In Fig. 7.5 we consider a Rician channel (5.9) with $\kappa = 5$, which describes a channel with a rich multipath environment and a significant LOS component. The CCDF of the penalty for the 2×2 ZF-MIMO system is shown in Fig. 7.5a for various values of ρ. Similar to Rayleigh channel, simulations show that the distribution γ_{ZF} is affected by ρ

and the slope of the distribution tails follows the 10dB-per-decade slope. In difference with the Rayleigh channel reduced path correlation can lead to both a penalty or a gain depending on the degree of correlation. It is not in scope of this report to fully study this effect but it may be subjected to further studies. As seen in Fig. 7.5b for SVD-MIMO system, there is a reduced probability of large penalties over the SISO system. The improvement also increases for lower values of ρ.

A comparison of the two MIMO systems, the SISO system and an additional MISO system are shown in Fig. 7.6. The Multiple-Input-Single-Output (MISO) is added as a reference as such systems are currently deployed in space diversity configurations [1, 2]. The penalty γ_{MISO} is equivalent to the least attenuation signal at the receiver which corresponds to the selective combining solution [8]. An interesting observation for the 2×2 MIMO system is that the distribution of γ_{ZF} closely follows the distribution of γ_{SISO}, and also the distribution of γ_{SVD} follows the distribution of γ_{MISO}. This is most likely due to the fact that the multipath fading can affect the channel orthogonality condition (3.9) and thus cause additional penalty.

For microwave links, the result of this section can be summarized as follows. For multipath fading, the results shows that slightly changed probability of outage can be expected for ZF system. This change in outage probability can be related to a average penalty offset. However, for SVD systems a general improvement of the outage probability can be expected.

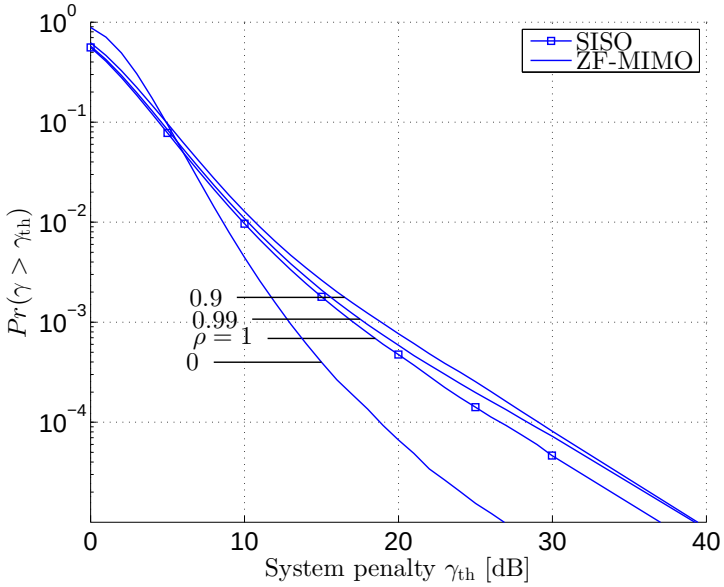

(a) System penalty CCDF for ZF-MIMO system.

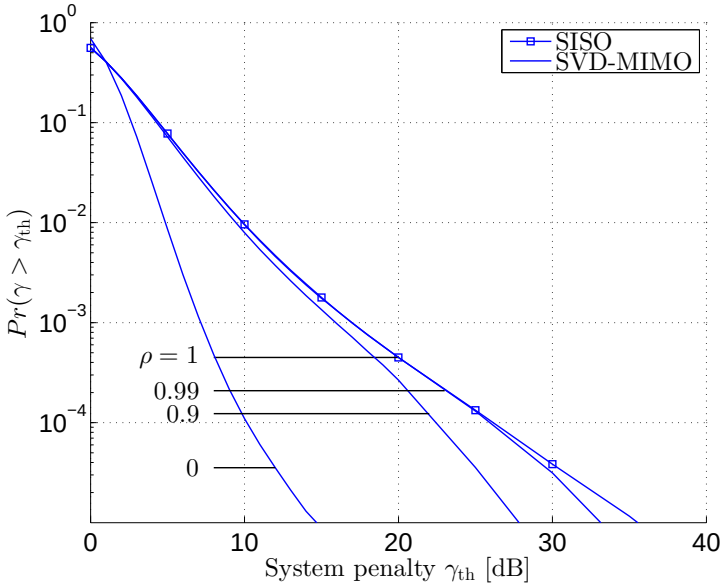

(b) System penalty CDF for SVD-MIMO system.

Figure 7.5: System penalty CCDF for ZF-MIMO and SVD-MIMO systems in correlated Rician channel for $\kappa = 5$ for several values of ρ.

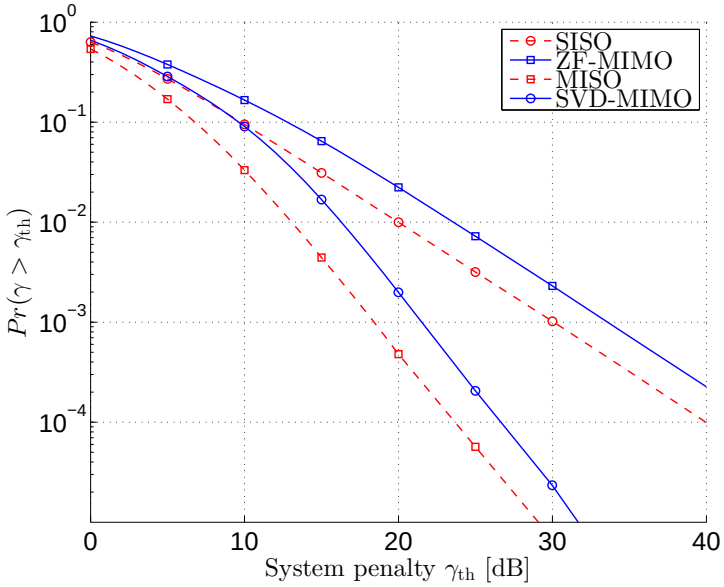

(a) System penalty CCDF in Rayleigh channel given $\rho = 0.9$

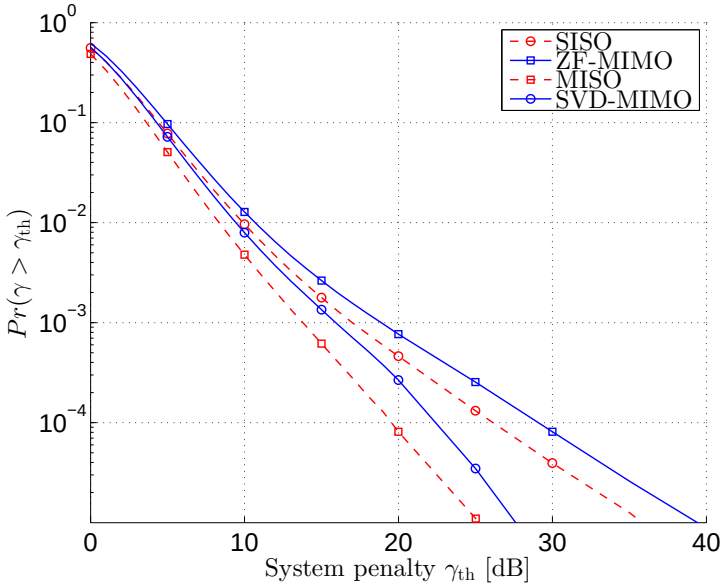

(b) System penalty CCDF in Rician channel given $\kappa = 5$ and $\rho = 0.9$

Figure 7.6: A comparison of the system penalty for all system in the Rayleigh and Rician channel.

7.3 Deployment Penalty in Fading Channels

This section is devoted to the study of consequences of sub-optimal deployment during deep fades. Recall the deployment conditions for determenistic channel $\mathbf{H}_{\text{LOS}}$, see (3.9) and (3.14). The Rayleigh and Rician distribution of (5.9) for $\kappa = 5$ is used to simulate the deep fade region.

Simulations have shown that for a correlated Rayleigh and Rician channels sub-optimal deployment ($\eta < 1$) translates to an average additional penalty. The deployment penalty plotted against η for the Rayleigh channel is given in Fig. 7.7. It reveals an increased penalty as η decreases, similar as the deployment penalty of a deterministic channel. It is noted that in an uncorrelated Rayleigh channel, $\rho = 0$, the system performance is independent of the deployment and thus the system experiences no extra penalty due to deployment. In practise this means channels with less correlated fading, such as severe refractive fading in LOS microwave links or in typical access channels, allows for smaller antenna separation.

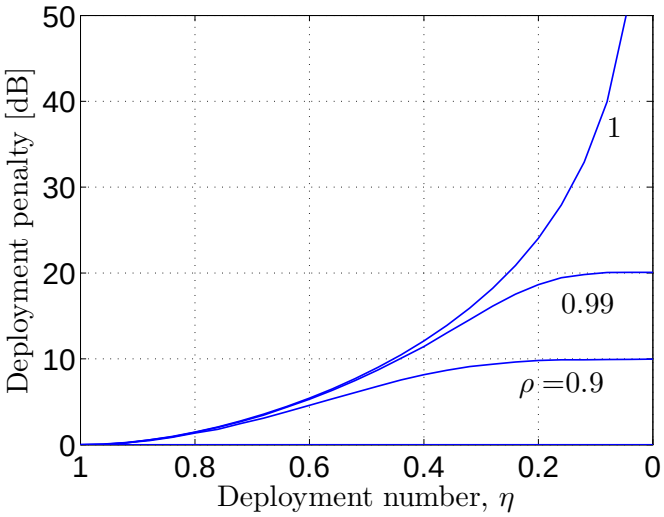

Figure 7.7: Additional ZF-MIMO deployment penalty in a Rayleigh channel against deployment number η for some correlation coefficients ρ.

It was shown in Fig. 3.3a in Chapter 3 that a deterministic LOS channel is subjected to a deployment penalty if the deployment is sub-optimal ($\eta < 1$). Since the Rician channel includes a deterministic component the deployment predicted to be higher than for a pure Rayleigh channel which is shown in Fig. 7.8.

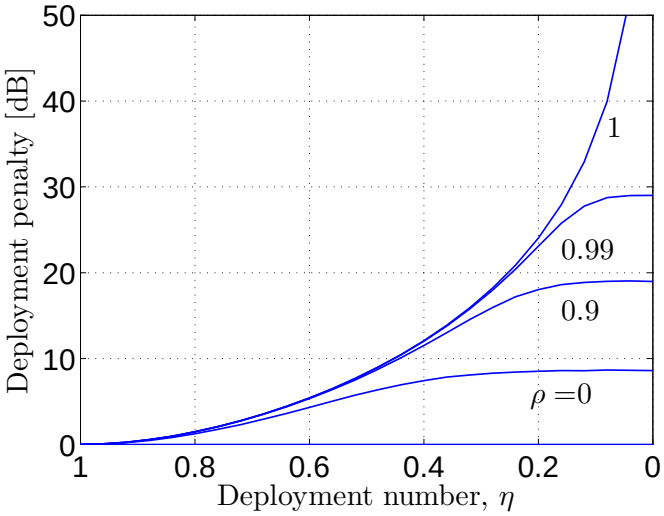

Figure 7.8: Additional ZF-MIMO deployment penalty in a Rician channel with $\kappa = 5$ against deployment number η for some correlation coefficients ρ.

8

Discussion

Channel models and performance prediction can be challenging to find for LOS microwave links if they should be both accurate and general in terms of deployment, frequency and hop length. Several different approaches have been proposed such as the ITU method or analytical models [2, 19]. All methods and models involve a trade-off between complexity, accuracy and how general they are.

For unobstructed links, two mechanisms have been found to affect the performance and cause outages, dominantly rain and refractivity related effects. As for most atmospheric effects the occurrence and severity of these mechanisms depends on climate, terrain, hop-length and frequency. In earlier works, including the ITU model for SISO links, rain fading is modelled as attenuation of the received signal [2]. From real-world MIMO measurements we found that rain attenuation can be assumed to be completely correlated between all MIMO paths. For rain fading under this assumption, all prediction methods for SISO links can directly be used for MIMO links.

Refractive fading on SISO links are usually modelled as multipath fading in combination with an additional frequency flat signal attenuation[2, 16, 22, 25]. Real-world measurements and prior studies show that the Rayleigh model and Rician model can also be used to describe multipath fading event for LOS MIMO links. It is expected from medium and long haul links that the fading may be frequency selective as well. A path correlation coefficient ρ is introduced to describe the correlation between the MIMO paths. It is reasonable that the correlation coefficient is a function of deployment, path length, frequency and fade depth. From measurements and studies on spatial diversity, the MIMO path correlation is expected to be high. This is a reasonable assumption since the spatial separation between MIMO paths are often small.

Simulations have shown that when calculating the outage probability for a MIMO link, uncorrelated fading among the MIMO paths can be statistically modelled as penalty/gain

offset when compared with a SISO link. This is true for a ZF receiver structure, similar as the prototype receiver used in the test links. Such a penalty/gains can be handled with an appropriate fade margin. For optimal system structure such as the SVD-MIMO system the probability of large system penalties are reduced, compared with a SISO system. This is likely due to the inherent diversity of the optimal systems. If the fading is fully correlated, it will result in an equal system penalty for both MIMO and SISO systems.

Given a frequency selective channel and an arbitrary receiver, it is difficult to accurately predict outage. In this case, the performance is dependent on the specific receiver. The method used for SISO systems is not easily applied to MIMO systems since the MIMO paths can have uncorrelated fading. In our long-term measurement, we did not capture any frequency selective fading in the two prototype links. This may have been because the multipath delay of the trial was too small to result in any in-band distortion. More measurements on longer frequency selective LOS-MIMO channel are needed to fully understand the dispersive fading on MIMO link. It is worth mentioning, simulations performed by [9] reveals that current linear MIMO equalizers are able to handle frequency selective fading but to a larger penalty than for a comparable SISO system. It is not in the scope of this report to derive a more general method to predict outage and performance on dispersive LOS-MIMO links.

Roughly speaking, MIMO systems can be divided into two different user cases: short haul, high frequency links, and long haul, low frequency links where available spectrum is limited. In both cases MIMO technology offers an excellent method to increase spectrum efficiency and throughput. For frequencies above 15-20GHz rain is the dominant fading. Rain attenuation increases rapidly with frequency and hop length, which limits the hop-length and upper frequency for any practical link. Lower frequency links are usually limited by refractive fading.

Short haul MIMO links have already successfully been deployed by Ericsson Research and the limiting rain fading is well understood from this report. It is likely that the increased spectral efficiency offered by MIMO technology will make the technology attractive for long-haul links in the future. While it should be possible to deploy a long haul MIMO link today, our understanding of the long haul MIMO channel is still limited and especially the impact of frequency selective fading. Moreover, a big drawback is also the large antenna separation needed for the deployment. Even though long-haul links might be less common it is still valuable to be able to predict the performance and hence further investigation is needed. The ITU model can, verified by measurement from real-world links and under the assumption of high correlation, most likely provide satisfactory predictions for most short to medium-haul links (<20km).

9

Conclusions

In this report we have studied prior work and performed real world measurements on LOS-MIMO microwave links to provide insights in fading characteristics and performance over LOS-MIMO microwave channels. From the work we have come to the following conclusions.

- We introduce a practical MIMO phase metric, $\Delta\theta$ (3.15) simply referred as MIMO phase and define an optimality criterion for 2×2 LOS-MIMO systems (3.17) that is equivalent to that in [5, 7].
- System penalty γ is defined in (3.22) and (3.25) as an equivalent to fade attenuation of a SISO system. Penalty is important for MIMO systems since not only the received power but also the structure of the MIMO channel affects performance.
- Motivated by measurements subjected to rain fading, rain is modelled as scalar attenuation of the nominal signal level for LOS-MIMO links. This results in an equivalent system penalty for both MIMO and SISO systems. Current rain fading prediction methods, such as those from ITU, can straightforwardly be applied on LOS-MIMO links.
- Predicted by the ITU method, the occurrence and severity and refractive fading increase with both geoclimatic factors, hop length and frequency. The method predict a 10dB-per-decade slope of deep fade probabilities for SISO systems as in Fig. 5.1
- Motivated by measurements subjected to short term refractive fading characteristics, a correlated Rician channel model (5.9) has been proposed.
- It is shown by simulations that in the deep fading region, the distribution of the penalty γ_{ZF} follows γ_{SISO} with a 10dB-per-decade slope, given the assumption of

Rayleigh/Rician channels.

- Reduced correlation leads to a penalty offset from the SISO system to the ZF-MIMO system when calculating outage probability.
- For a SVD-MIMO system a general improvement of outage probabilities can be expected to outperform a SISO system. The improvement increases for decreased ρ.
- Sub-optimal antenna deployment causes an additional system penalty as in Fig. 3.3a. In Rayleigh/Rician fading channels the average additional penalty during deep fades is related to the correlation of the MIMO paths. Reduced correlation leads to smaller average additional deployment penalty.

9.1 Further Studies

Exhaustive studies are still required to fully understand fading mechanisms in microwave LOS-MIMO channels. Especially, fading correlation and frequency selective fading are not fully investigated. More measurements and experiments on real links needs to be performed to capture these effects. Given limited measurements, simulations have been performed but more can be done also in this area. We have seen from simulations that the choice of system structure can have large impact on the performance in the deep fading region.

One of the key goals of this work was to investigate performance over LOS-MIMO channels and if possible, suggest relevant modifications of the existing standards, such as ITU models. To further increase the understanding of the topics, we will highlight some areas that can be investigated in more details.

- The study of correlated fading in Rayleigh/Rician channels, and its impact on system performance and outage probabilities will be useful.
- More studies are required on correlation and frequency selectivity in LOS-MIMO channels in terms of distance, deployment, frequency etc. Measurements from real-world links are useful to characterize these effects and enrich the propagation models.
- Based on increased knowledge of the channel, studies on efficient receiver structures, in terms of complexity and performance, in correlated frequency selective MIMO channels are useful.

Bibliography

[1] A. Käse, Radio Path Planning Handbook, Ericsson GmbH, 2006.

[2] International Telecommunication Union, ITU-R Recommendation P.530-14, Propagation data and prediction methods required for the designof terrestrial line-of-sight systems (2012).

[3] T. Manning, Microwave radio transmission design guide, Artech House, 2009.

[4] F. Bohagen, P. Orten, G. Oien, Modeling and analysis of a 40 ghz mimo system for fixed wireless access, in: Vehicular Technology Conference, 2005. VTC 2005-Spring. 2005 IEEE 61st, Vol. 3, 2005, pp. 1691–1695 Vol. 3.

[5] D. Gesbert, H. Bolcskei, D. A. Gore, A. J. Paulraj, Outdoor mimo wireless channels: Models and performance prediction, IEEE Transactions on Communications 50 (12) (2002) 1926–1934.

[6] D. Tse, Fundamentals of wireless communication, Cambridge university press, 2005.

[7] F. Bohagen, P. Orten, G. E. Oien, Design of optimal high-rank line-of-sight mimo channels, Wireless Communications, IEEE Transactions on 6 (4) (2007) 1420–1425.

[8] A. Goldsmith, Wireless communications, Cambridge university press, 2005.

[9] T. Ingason, H. Liu, Line-of-sight mimo for microwave links-adaptive dual polarized and spatially separated systems, Master's thesis, Chalmers University of Technology (2009).

[10] International Telecommunication Union, ITU-R Recommendation P.838-3,Specific attenuation model for rain for use in prediction methods (2005).

[11] H. Xu, T. S. Rappaport, R. J. Boyle, J. H. Schaffner, Measurements and models for 38-ghz point-to-multipoint radiowave propagation, IEEE Journal on Selected Areas in Communications 18 (3) (2000) 310–321.

[12] International Telecommunication Union, ITU-R Recommendation P.453-10, The radio refractive index: its formula and refractivity data (2012).

[13] B. Bean, E. Dutton, Radio meteorology. national bureau of standards monogr (1968).

[14] M. Grabner, V. Kvicera, Atmospheric refraction and propagation in lower troposphere, Electromagnetic Waves (2011) 139–156.

[15] I. Sirkova, M. Mikhalev, Influence of tropospheric duct parameters changes on microwave path loss, in: Proceedings of the XXXVIII International Scientific Conference on Information, Communication & Energy Systems & Technologies, ICEST, 2003, pp. 16–18.

[16] M. Shafi, Statistical analysis/simulation of a three ray model for multipath fading with applications to outage prediction, IEEE Journal on Selected Areas in Communications 5 (3) (1987) 389–401.

[17] E. Costa, The effects of ground-reflected rays and atmospheric inhomogeneities on multipath fading, IEEE Transactions on Antennas and Propagation 39 (6) (1991) 740–745.

[18] M. Thompson Jr, H. Janes, Measurements of phase stability over a low-level tropospheric path, J. Research Natl. Bur. Standards D 63 (1959) 45.

[19] P. Almers, E. Bonek, A. Burr, N. Czink, M. Debbah, V. Degli-Esposti, H. Hofstetter, P. Kyö, D. Laurenson, G. Matz, et al., Survey of channel and radio propagation models for wireless mimo systems, EURASIP Journal on Wireless Communications and Networking 2007.

[20] A. Vigants, Space-diversity performance as a function of antenna separation, IEEE Transactions on Communication Technology 16 (6) (1968) 831–836.

[21] T. Lee, S. Lin, A model of space diversity for microwave radio against thermal noise caused outage during multipath fading, in: IEEE Global Telecommunications Conference, 1988, and Exhibition.'Communications for the Information Age.'Conference Record, GLOBECOM'88., IEEE, 1988, pp. 1440–1446.

[22] K. Pearson, Method for the prediction of the fading performance of a multisection microwave link, Proceedings of the Institution of Electrical Engineers 112 (7) (1965) 1291–1300.

[23] W. Barnett, Multipath propagation at 4, 6, and 11 ghz, Bell System Technical Journal 51 (2) (1972) 321–361.

[24] R. G. McKay, M. Shafi, Multipath propagation measurements on an overwater path in new zealand, IEEE Transactions on Communications 36 (7) (1988) 781–788.

[25] W. Rummler, A new selective fading model: Application to propagation data, Bell system technical journal 58 (5) (1979) 1037–1071.

[26] F. Bøhagen, Modeling, characterization and design of line-of-sight wireless mimo channels, Ph.D. thesis, University of Oslo (2007).

[27] Experimental results on phase measurement of 2×2 microwave line-of-sight mimo links, Ericsson Internal Report.

[28] S.-F. Ong, C.-F. Hu, Propagation measurements on an over-water, line-of-sight link in singapore, in: Proceedings of 1997 International Conference on Information, Communications and Signal Processing, 1997. ICICS., Vol. 3, 1997, pp. 1714–1718 vol.3.